UNIVERSITY OF CALIFORNIA, SAN DIEGO

Magnetically Vectored Nanocapsules for Tumor Penetration and Remotely Switchable On-Demand Drug Release

A dissertation submitted in partial satisfaction of the

requirements for the degree Doctor of Philosophy

in

Materials Science and Engineering

by

Seong Deok Kong

Committee in Charge:

Professor Sungho Jin, Chair
Professor Prabhakar Bandaru
Professor Vlado A. Lubarda
Professor Marc Meyers
Professor Yu Qiao

2010

The dissertation of Seong Deok Kong is approved, and it is acceptable in quality and form for publication on microfilm and electronically:

_____

_____

_____

_____

_____

Chair

University of California, San Diego

2010

Dedicated to

my wife

“ Blessed is the one who does not walk in step with the wicked or stand in the way that sinners take or sit in the company of mockers, but whose delight is in the law of the LORD, and who meditates on his law day and night. That person is like a tree planted by streams of water, which yields its fruit in season and whose leaf does not wither whatever they do prospers. Not so the wicked! They are like chaff that the wind blows away. Therefore the wicked will not stand in the judgment, nor sinners in the assembly of the righteous. For the LORD watches over the way of the righteous, but the way of the wicked leads to destruction.”

Psalm 1

TABLE OF CONTENTS

LIST OF FIGURES

LIST OF TABLES

ACKNOWLEDGEMENTS

I really thank God for allowing me to achieve these tremendous works and finish my Ph.D. How gracious He is! “God did it!!!”

I wish to acknowledge and deeply thank my advisors, Professor Sungho Jin for his strong encouragement, support, and guidance during the course of this research. I wish to express my gratefulness to my committee members for their time and helpful suggestions: Professor Prabhakar Bandaru, Professor Valdo A. Lubarda, Professor Marc Meyers, and Professor Yu Qiao.

Chapter 2 and 3, in full, have been submitted for publication, “Magnetically Vectored Nanocapsules for Tumor Penetraion and Remotely Switchable On-Demand Drug Release”, by Seong Deok Kong, Weizhou Zhang, Jun Hee Lee, Karla Brammer, Ratnesh Lal, Michael Karin, and Sungho Jin.

I would also like to recognize and thank the following individuals for their assistance in various aspects of this work: Dr. Leon Chen, Dr. Brian Oh, Dr. Chris Hong, Dr. Edward Kim, Dr. Eric Kim, Dr. David Kim, Dr. Mariana Loya, Dr. Lisa Chamberlain, Karla Brammer, Kevin Noh, Michael Oh, Christine Frandsen, Laura Connelly, Stanley Kim, Garrett Smith, Jeanne Khamwannah, and Du Young Choi. I appreciate all the helps from my collaborators. We have shared the joy and frustration together solving countless materials, fabrications and device problems in the past several years.

Special thanks go to Charlotte Lauve for taking care of the administrative burdens for me.

Finally, I wish to thank my wife, my parents, my parents-in-law, my son, my daughter, and other family members for their prayers and lovely encouragement during this time. Thanks again to my wife, Ha Ram Kim, for her best support for my effort toward the Ph.D degree.

I also wish to thank my many friends and other colleagues who are too numerous to mention all by name.

VITA

1973	Born in Seoul, South Korea
2000	B.S., Chemistry, Kyunghee University, South Korea
2002	M.S., Chemistry, Yonsei University, South Korea
2010	Ph.D., Materials Science and Engineering, University of California, San Diego

SELECTED AWARDS

Awarded with the Materials Science Research Assistant Fellowship,
University of California, San Diego for the year 2004-2010

Awarded with the National Research Lab (NRL) Scholarship,
Korea Institute Science and Technology, Korea for the year 2000-2001.

PUBLICATIONS

Journals Articles:

1. "BBB crossing and Drug Delivery using Magnetic Nanoparticles", **Seong Deok Kong**, Jisook Lee, Brian Eliceiri, Sungho Jin, in preparation
2. "Control Drug Release from Lipid-polymer hybrid Nanocapsule by External Magnetic Field" **Seong Deok Kong**, Marta Sator, Liangfang Zhang, Sungho Jin, in preparation
3. "Nanotoxicity in Brain Tissue with surface-functionalized Iron Oxide Nanoparticles", **Seong Deok Kong**, Youngsoon Kim, Veronica Shubayev, Sungho Jin, in preparation
4. "Magnetically Vectored Nanocapsules for Tumor Penetration and Remotely Switchable On-Demand Drug Release", **Seong Deok Kong**, Weizhou Zhang, Jung Hee Lee, Karla Brammer, Ratnesh Lal, Michael Karin, and Sungho Jin, submitted
5. "pH-Sensitive, *N*-Ethoxybenzylimidazole (NEBI) Bifunctional Crosslinkers Enable Triggered Release of Therapeutics from Drug Delivery Carriers" Alice Luong, Tawny Issarapanichkit, **Seong Deok Kong**, Rina Fong, and Jerry Yang Org. Biomol. Chem., 2010, in press
6. "Antibiofouling, Sustained Antibiotic Release by Si Nanowire Templates", Karla S. Brammer, Chulmin Choi, Seunghan Oh, Christine J. Cobb, Laura S. Connelly, Mariana Loya, **Seong Deok Kong**, and Sungho Jin, Nano Lett., 9(10), 3570 (2009)
7. "Acidic Hydrolysis of N-Ethoxybenzylimidazoles (NEBIs): Potential Applications as pH-Sensitive Linkers for Drug Delivery.", **Seong Deok Kong**, Alice Luong, Gerald Manorek , Stephen B. Howell, Jerry Yang, Bioconjugate Chem., 18(2), 293 (2007)
8. "Friedel-Crafts type alkylation of 1,2,3,4,5,6,7,8-octahydroanthracene with vinylchlorosilanes: synthesis of mono, bis[2-(chlorosilyl)ethyl]-1,2,3,4,5,6,7,8-octahydroanthracenes", **Seong Deok Kong** , Chang Yeob Lee, Bok Ryul Yoo, Myong Euy Lee, Il Nam Jung, Bulletin of the Korean Chemical Society, 23(9), 1213 (2002)
9. " One-Step Synthesis of Fluorenyl-Substituted Chlorosilanes: Friedel-Crafts Type Cycloalkylation of Biphenyl with (Dichloroalkyl)silane", Young-Sang Song, **Seong Deok Kong**, Shah Alam Khan, Bok Ryul Yoo, Il Nam Jung Organometallics, 20(26), 5586, (2001)

Patents / Technology disclosures:

1. Jin, Sungho; Brammer, Karla; Oh, Seunghan; **Kong, Seong Deok**, "Switchable nano-vehicle delivery systems, and methods for making and using them", PCT Int. Appl. (2009)
2. Yang, Jerry; **Kong, Seong Deok**; Luong, Alice; Howell, Stephen, "Acid-sensitive linkers, N-alkoxyalkylimidazoles, for using in prodrugs for controlled drug delivery in the cancer treatment, as well as imaging agents", PCT Int. Appl. (2007)
3. Jung, Il Nam; Yoo, Bok Ryul; Han, Joon Soo; Kim, Jeong Hyun; **Kong, Seong Deok**, "A Preparation Method of Organochlorosilanes by Reductive Deoxysilation Reaction of Aldehydes or Ketones", Korean Patent 0487904 (2005. 4. 27)

Proceedings and Conference Presentation:

1. **Kong, Seong Deok**; Lee, Jun Hee; Zhang, Weizhou; Karin, Michael; Jin, Sungho. "Magnetically vectored delivery of cancer drugs using remotely on-off switchable nanospheres." 240th ACS National Meeting, Boston, MA, United States, August 22-26, 2010 (2010)
2. Luong, Alice; **Kong, Seong Deok**; Fong, Rina; Lin, Lynnie; Issarapanichkit, Tawny; Yang, Jerry, "Exploring pH-sensitive NEBI linkers for cancer drug delivery applications." 235th ACS National Meeting, New Orleans, LA, United States, April 6-10, 2008 (2008)
3. Luong, Alice; **Kong, Seong Deok**; Manorek, Gerald; Howell, Stephen B.; Yang, Jerry, "*N*-Ethoxybenzylimidazoles: pH Sensitive Linkers for Controlled Release of Cancer Therapeutics", 41st Western Regional Meeting of the American Chemical Society, San Diego, CA, United States, October 9-13 (2007)
4. **Kong, Seong Deok**; Luong, Alice; Yang, Jerry, "*N*-Ethoxybenzylimidazoles as Potential pH-Sensitive Linkers for Drug Delivery", 41st Western Regional Meeting of the American Chemical Society, San Diego, CA, United States, October 9-13 (2007)
5. Luong, Alice; **Kong, Seong Deok**; Manorek, Gerald; Howell, Stephen B.; Yang, Jerry, "*N*-Ethoxybenzylimidazoles: pH Sensitive linkers for controlled release of cancer therapeutics", 234th ACS National Meeting, Boston, MA, United States, August 19-23, 2007 (2007)
6. **Kong, Seong Deok**; Luong, Alice; Yang, Jerry, "Acidic hydrolysis of *N*-ethoxybenzylimidazoles: Potential applications as pH-sensitive linkers for drug delivery", 232nd ACS National Meeting, San Francisco, CA, United States, Sept. 10-14, 2006 (2006)

ABSTRACT OF THE DISSERTATION

Magnetically Vectored Nanocapsules for Tumor Penetration and
Remotely Switchable On-Demand Drug Release

by

Seong Deok Kong

Doctor of Philosophy in Materials Science and Engineering

University of California, San Diego, 2010

Professor Sungho Jin, Chair

Hollow-sphere nanocapsules containing intentionally trapped magnetic nanoparticles and defined anticancer drugs provide a powerful magnetic vector under moderate gradient magnetic fields, and enable the nanocapsules to penetrate into the midst of tumors and allow a controlled on-off switchable release of the anticancer drug cargo by remotely applied Radio Frequency (RF) magnetic field. This imageable smart drug delivery system is compact because the drug molecules and magnetic nanoparticles can all be self-contained within 80~150 nm capsules. *In vitro* as well as *in vivo* results indicate that the nanocapsules are effective in reducing tumor cell growth.

In Chapter 1, the concept of Drug Delivery Systems (DDSs) and the impact of nanotechnology on Drug Delivery Systems were introduced. Triggered drug release using magnetothermally-responsive nanomaterials, magnetic nanoparticles for nanomedicine,

and ordered mesoporous materials in the context of Drug Delivery System were discussed. In Chapter 2, creation of remotely controllable, On-Off switchable drug release methodology was described. In this thesis work, triggerable nanocapsules which contain magnetic nanoparticles responsive to external radio frequency (RF) magnetic field have been successfully created. This is in contrast to the regular hollow nanospheres for slow passive release of drugs. The new nanocapsule material consists of bio-inert, bio-compatible or bio-degradable material that we can be selected from a variety of materials depending on specific medical applications. In Chapter 3, study and utilization of magnetic vector for guided tumor penetration was discussed. In the presence of a moderate gradient magnetic field, a powerful magnetic vector is created that allows these nanocapsules to cross cell membranes or blood-tissue barriers and penetrate into the midst of tumors, thus overcoming the well-known problem of limited access of anti-cancer drugs to cancer cells in the interior of a tumor tissue. In Chapter 4, potential applications to Blood-Brain-Barrier (BBB) crossing and other therapeutics was described. In Chapter 5, the study was summarized and concluded.

Chapter 1.

Introduction

1.1. Drug Delivery Systems

Drug delivery systems are formulations or devices that enable the introduction of a therapeutic substance in the body and improve its efficacy and safety by controlling the rate, time, and place of release of drugs in the body (*1*). Drug delivery systems can improve the pharmacological properties of free drugs using particulate carriers, composed primarily of lipids and polymers (*2*). Drug delivery systems may involve enhanced bioavailability, improved therapeutic index, or improved patient acceptance or compliance.

Drug Delivery Systems are designed to consider drug properties such as potency, stability, solubility, size, and charge. Polymer conjugated Drug Delivery Systems which can carry small amount of molecules needs drugs with higher potencies to deliver therapeutically effective amount of drugs (*3*). Contrastively, because liposome can entrap large amount of therapeutic molecules, drug potency is less considerable for this carrier (*4*). However, the size of therapeutic molecules is also very important issue for Drug Delivery Systems. Even the high capacity of liposomes becomes problematic for proteins

which are large size molecules. Because drug solubility may be a limiting factor for drug retention, it can be also an important consideration in Drug Delivery System. Hydrophilic drugs can be readily delivered with carrier-drug conjugates, but hydrophobic drugs need the intermediate between hydrophobic drugs and hydrophilic media of bodies (*5*).

A schematic illustration (Figure 1) illustrates the passive or ligand-targeted accumulation of Drug Delivery Systems in breast cancer tumors through the Enhanced Permeability and Retention (EPR) effect (*6*). Drug Delivery Systems containing an anticancer molecule are injected through blood vessel, and extravasated from the blood through the leaky endothelial cells and accumulated in tumor tissue (dark green in Figure 1 A). The therapeutic molecules are released from Drug Delivery Systems by two different environments: (a) the molecules are released at extracellular environment and taken up into the cells. (b) Ligand-targeted Drug Delivery Systems containing anticancer molecules bind to cell surface receptors which can internalize Drug Delivery Systems into endosomes and the anticancer molecules escape the endosomes and perform its intracellular action (*2*).

Table 1 summarized the non-ideal properties of free drugs and their therapeutic implication. Drug delivery systems (DDSs) provide the ideal properties to maximize the therapeutic efficacy with free drugs. For example, the poor solubility of hydrophobic drugs (most of pharmaceutical drugs are hydrophobic.) makes them precipitate in aqueous media in the body. Using drug delivery system such as lipid micelles or liposomes provides both hydrophobic and hydrophilic environment, enhancing drug solubility. Drug delivery systems decrease the tissue toxicity and side effect. Drug

delivery systems also protect the drug from premature degradation and functions and reduce clearance.

Drug delivery systems can increase drug concentrations in disease tissues such as tumor through a triggered release mechanism-by changes in pH, temperature, or magnetic fields or by engineered sensitivities to biocompatible chemicals and enzymes, light, or radiofrequency (*7, 8*).

Table 2 shows some examples of drug delivery systems that have received regulatory approval. Various radioimmunopharmaceuticals, innumoxoxins, and immunoconjugates are on the market. A signaling antibody as a targeting moiety gives a significant advantage of the possibility of additive or synergistic activities for drug delivery systems. The passive-targeting effect can substantially enhance the amount of drugs at disease sites such as tumors and sites of infection and inflammation (*2*).

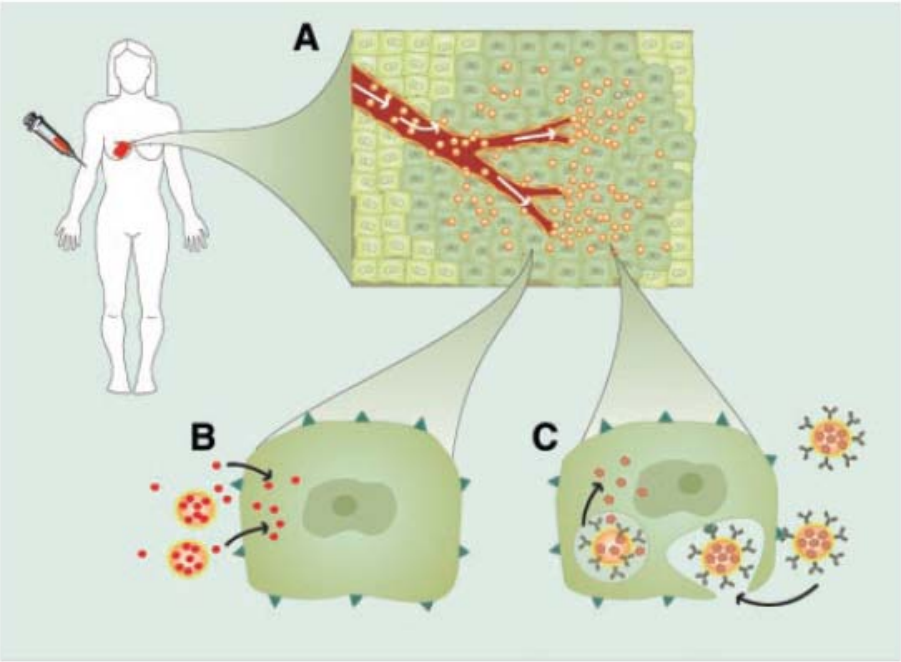

Figure 1. Schematic illustration showing the passive or ligand-targeted accumulation of Drug Delivery System in breast cancer tumors through the Enhanced Permeability and Retention (EPR) effect(*2*).

Table 1. Non-ideal properties of drugs and their therapeutic implications (*2*).

Table 1. Non-ideal properties of drugs and their therapeutic implications.

Problem	Implication	Effect of DDS
Poor solubility	A convenient pharmaceutical format is difficult to achieve, as hydrophobic drugs may precipitate in aqueous media. Toxicities are associated with the use of excipients such as Cremphor (the solubilizer for paclitaxel in Taxol).	DDS such as lipid micelles or liposomes provide both hydrophilic and hydrophobic environments, enhancing drug solubility.
Tissue damage on extravasation	Inadvertent extravasation of cytotoxic drugs leads to tissue damage, e.g., tissue necrosis with free doxorubicin.	Regulated drug release from the DDS can reduce or eliminate tissue damage on accidental extravasation.
Rapid breakdown of the drug in vivo	Loss of activity of the drug follows administration, e.g., loss of activity of camptothecins at physiological pH.	DDS protects the drug from premature degradation and functions as a sustained release system. Lower doses of drug are required.
Unfavorable pharmacokinetics	Drug is cleared too rapidly, by the kidney, for example, requiring high doses or continuous infusion.	DDS can substantially alter the PK of the drug and reduce clearance. Rapid renal clearance of small molecules is avoided.
Poor biodistribution	Drugs that have widespread distribution in the body can affect normal tissues, resulting in dose-limiting side effects, such as the cardiac toxicity of doxorubicin.	The particulate nature of DDS lowers the volume of distribution and helps to reduce side effects in sensitive, nontarget tissues.
Lack of selectivity for target tissues	Distribution of the drug to normal tissues leads to side effects that restrict the amount of drug that can be administered. Low concentrations of drugs in target tissues will result in suboptimal therapeutic effects.	DDS can increase drug concentrations in diseased tissues such as tumors by the EPR effect. Ligand-mediated targeting of the DDS can further improve drug specificity.

Table 2. Examples of Drug delivery systems that have received regulatory approval. Years given are for the United States, unless otherwise specified.

Drug or therapeutic agent (trade name), manufacturer(s)	Indication	Year of approval
Liposomal amphotericin B (AmBisome), Gilead, Fujisawa	Fungal infections	1990 (Europe), 1997
	Leishmaniasis	2000
PEG-adenosine deaminase (Adagen), Enzon	Severe combined immunodeficiency disease	1990
Styrene maleic acid and neocarzinostatin copolymer in Ethiodol (SMANCS/Lipiodol, Zinostatin stimalamer), Yamanouchi	Hepatocellular carcinoma	1993 (Japan) 1996 (Japan)
Stealth (PEG-stabilized) liposomal doxorubicin (Doxil/Caelyx), ALZA, Schering Plough	Kaposi's sarcoma	1995
	Refractory ovarian cancer	1999
	Refractory breast cancer	2003 (Europe, Canada)
Liposomal cytosine arabinoside (DepoCyt), SkyePharma	Lymphomatous meningitis	1999
	Neoplastic meningitis	Phase IV
Denileukin diftitox or interleukin 2–diptheria toxin fusion protein (ONTAK), Seragen	Cutaneous T-cell lymphoma	1999
Liposomal doxorubicin (Myocet), Elan	Metastatic breast cancer in combination with cyclophosphamide	2000 (Europe)
Gemtuzumab ozogamicin or anti-CD33–linked calicheamicin (Mylotarg), Wyeth-Ayerst	$CD33^+$ relapsed acute myeloid leukemia	2000
Liposomal verteporfin (Visudyne), QLT, Novartis	Wet macular degeneration in conjunction with laser treatment	2000 2001 2003 (Japan)
PEG-interferon α-2b (PEG-Intron), Enzon, Schering-Plough	Hepatitis C	2001
PEG–granulocyte colony stimulating factor or pegfilgrastim, (Neulasta), Amgen	Reduction of febrile neutropenia associated with chemotherapy	2002
^{90}Y-ibritumomab tiuxetan or ^{90}Y anti-CD20 (Zevalin), IDEC	Relapsed or refractory non-Hodgkin's lymphoma	2002
^{131}I-tositumomab (anti-CD20) (Bexxar), Corixa, GlaxoSmithKline	$CD20^+$ relapsed non-Hodgkin's lymphoma	2003

1.2. Impact of Nanotechnology on Drug Delivery

The application of nanotechnology toward drug delivery is widely expected to achieve (a) improved delivery of poorly water-soluble drugs, (b) targeted delivery of drugs in a cell- or tissue-specific manner, (c) transcytosis of drugs across tight epithelial and endothelial barriers, (d) delivery of large macromolecule drugs to intracellular sites of action, (e) co-delivery of two or more drugs or therapeutic modality for combination therapy, (f) visualization of sites of drug delivery by combining therapeutic agents with imaging modalities, and (g) real-time read on the *in vivo* efficacy of a therapeutic agent (*9*).

Liposomes were the first nanotechnology drug delivery systems based on lipids in 1960s (*10*). Subsequently, the controlled release polymer system for delivery of macromolecules was reported in 1976 (*11*). More complex drug delivery systems which responded to change of pH to trigger drug release (*12*) and targeted to specific cells were described in 1980 (*13, 14*). The stealth liposomes which have long circulating time were described in 1987 (*15*). Polyethylene glycol (PEG) increased circulation times for liposomes (*16*) and polymeric nanoparticles (*17*) in 1990 and 1994, respectively. Liposomal drugs and polymer-drug conjugates which improve the pharmaceutical efficacy or dosing of clinical approved drugs are two dominant classes among the first generation products.

In order to develop the current clinically approved nanotechnology products, many parameters are considered for the successful development and manufacturing of targeted drug delivery vehicles including (a) the use of biocompatible materials with simple robust processes for biomaterial assembly, conjugation chemistry, and purification

steps; (b) the ability to optimize in parallel the myriad of biophysicochemical parameters of targeted drug delivery vehicles important for pharmacokinetic properties and possible cell uptake; and (c) developing scalable unit operations amenable to manufacturing large quantities of targeted drug delivery systems needed for clinical translation. Figure 2 shows that the efficacy of nanoparticles as delivery vehicles is highly size- and shape-dependent. The size of the nanoparticles affects their movement in and out of the vasculature, whereas the margination of particles to vessel wall is impacted by their shape (*9*).

After particles extravasate out of the vasculature into the tumor tissue by Enhanced permeability and retention (EPR) effects, specific uptake by cancer cells is facilitated by active targeting and receptor-mediated endocytosis (Figure 3). Figure 3 presents passive *vs* active targeting: (Right) Particles tend to passively extravasate through the leaky vasculature, which is characteristic of solid tumors and inflamed tissue, and preferentially accumulate through the Enhanced permeability and retention (EPR) effect. In this case, the drug may be released in the extracellular matrix and diffuse throughout the tissue for bioactivity. (Middle) Once particles have extravasated in the target tissue, the presence of ligands on the particle surface can result in active targeting of particles to receptors that are present on target cell or tissue resulting in enhanced accumulation and cell uptake through receptor-mediated endocytosis. This process, referred to as “active targeting”, can enhance the therapeutic efficacy of drugs, especially those which do not readily permeate the cell membrane and require an intracellular site of action for bioactivity. (Left) The particles can be engineered for vascular targeting by incorporating ligands that bind to endothelial cell-surface receptors. While the presence

of leaky vasculature is not required for vascular targeting, when present as is the case in tumors and inflamed, this strategy may potentially work synergistically for drug delivery to target both the vascular tissue and target cells within the diseased tissue for enhanced therapeutic (9).

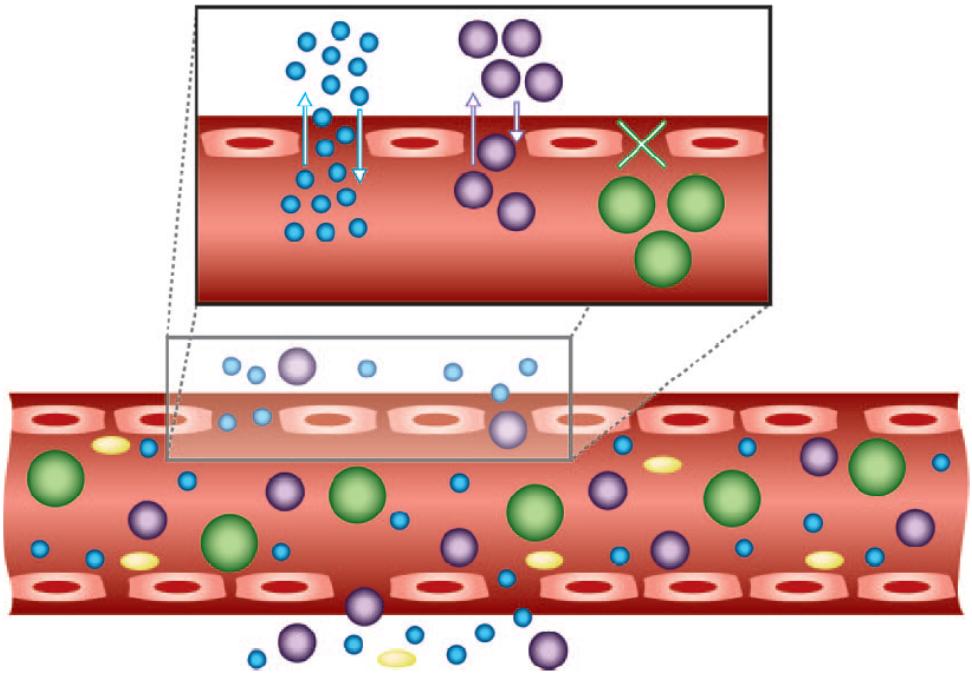

Figure 2. Efficacy of nanoparticles as delivery vehicles is highly size- and shape-dependent(*9*).

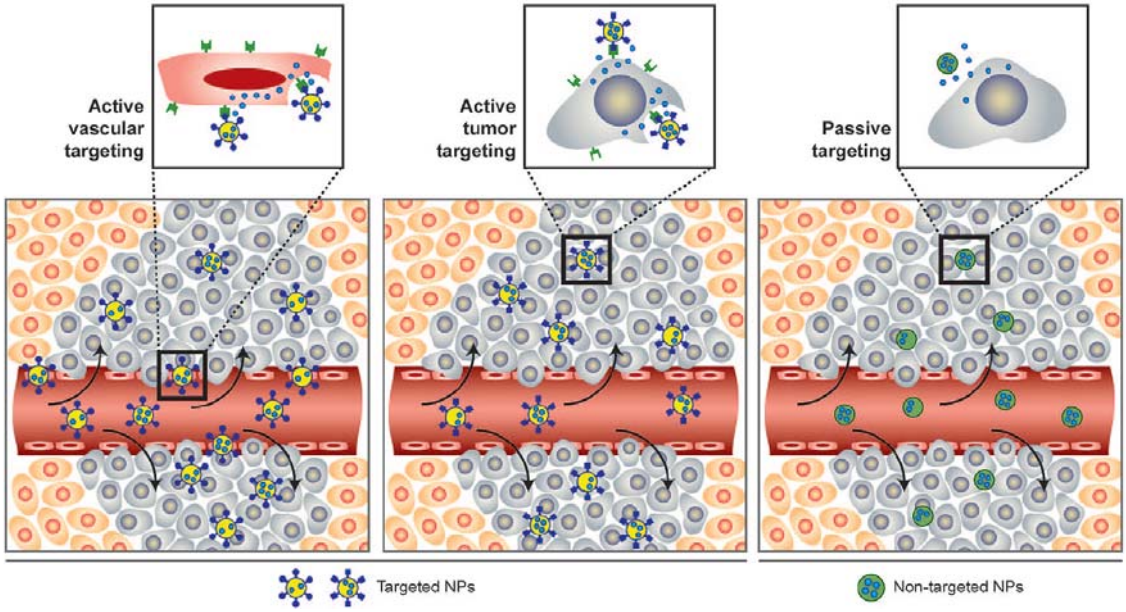

Figure 3. Passive *vs* active targeting (*9*).

1.3. Triggered Drug Release using Magnetothermally-responsive Nanomaterials

Externally triggered drug release is a highly desired mean for drug delivery systems. Specially, magnetothermally-triggered drug delivery systems can release drugs by external stimulus, alternating current (AC) magnetic field, to the body. The controlling drug release offers the benefit to patient by reducing the total amount of drugs required to reach an effective dose, reducing the frequency of administration, and assisting in sophisticated devices that include targeting, imaging and multiple modes of therapy (*18*).

Magnetically triggered release can be achieved by the oscillatory motion of magnets to mechanically open polymers resulting in drug diffusion (*19*), or magnetic heating of nanoparticles to give stimulus to thermally-responsive polymer (*20*). These methods for magnetically-triggered releases are used for several biomedical and biological applications. Superparamagnetic iron oxide nsnoparticles can be combined with a biodegradable gel to prolong the local delivery of dexamethasone as an anti-inflammatory agent (*21*). Magnetic nanoparticles can be also used in tissue engineering by attaching to cell membranes and applying an oscillating field to condition the cells for tissue growth (*22*).

Figure 4 shows magnetothermal responsive drug delivery systems using hydrogel structure. Magnetic nanoparticles are represented by rectangles, molecularly dispersed drug by circles, and thermoresponsive grafts are shown attached to the base network in the third depiction. Magnetic nanoparticles designed with the proper composition and size to accomplish heating using an alternating current (AC) magnetic field place the interior of thermally-responsive hydrogel and the pores of hydrogel are opened to release drugs, once heated. The nanoparticles are embedded directly in polymer or self-

assembled to encapsulate nanoparticles resulting in new structures such as micells, liposomes, or polymersomes (*23, 24*).

The properties of both the particles and the applied field influence the heating of magnetic nanoparticles. Figure 5 shows the device to create an alternating current (AC) magnetic field using electric coil to focus the magnetic field within. Thermal infrared images are shown to collect temperature data (Figure 5 b). In most case, higher field intensities generate more heat (Figure 6 shows more efficient heat as the field intensity is increased from 127 to 634 Gauss.) (*25*). In order to generate heat with alternating current (AC) magnetic field, the applied frequency is very important (the usual range of pulsed frequencies to generate heat is from 50 kHz to 10 MHz.).

Carrier selection and design are very important to the development of magnetothermally-triggered systems. In order to use magnetic nanoparticles as localized heat source for controlled-drug release, carrier should be heat-responded materials designed to phase separate or change conformations when heated. For example, polymers displaying a lower critical solution temperature (LCST) in aqueous solutions have been investigated by numerous researchers for thermo-sensitive drug delivery (*26, 27*). Poly(*N*-isopropylacrylamide) (PNIPAAm) is the most popular polymer which has 32 °C of lower critical solution temperature (LCST) for phase separation in water. Hydrogels based on PNIPAAm can entrap drugs and release drugs at the target site by swelling controlled release or squeezing controlled release with magnetic nanoparticles exposed to alternating current (AC) magnetic field (Figure 7).

The hyperthermia as a cancer treatment technique has been using the application of heat to preferentially kill cancer cells while having a lesser effect on healthy cells with

magnetic fluid (*28*). The temperature for hyperthermia is about 45 °C, as higher temperature causes whole cell necrosis in both healthy tissue and cancerous tumors (*18*). The first investigation of magnetic fluid hyperthermia treatment using magnetic nanoparticles to be heated by an alternating current (AC) magnetic field was by Gilchrist *et al.* in 1957 (*29*). Each magnetic nanoparticle (superparamagnetic nanoparticles which sizes are typically below 10 nm) is heated by applied field through the mechanism of Neel relaxation or rotation of the magnetization. Using the targeted ligands which conjugate the receptors overexpressed in many types of cancer cells, magnetic nanoparticles are localized at the cancerous tissue and then give heat to localized small tissue and potentially even individual cells by external magnetic field. Table 3 summarized the types of magnetic nanoparticles studied for hyperthermia.

For cancer diagnostics, Magnetic Resonance Imaging (MRI) is one of the most important tools and the standard clinical test to determine the presence, location, and size of a tumor, as the T2 relaxation mode allows distinction between normal soft tissue and the more rigid tissue which represents a tumor. Magnetic nanoparticles are the standard contrast agents used to improve imaging and also the therapeutic agent with hyperthermia treatment which is mentioned above (*30, 31*).

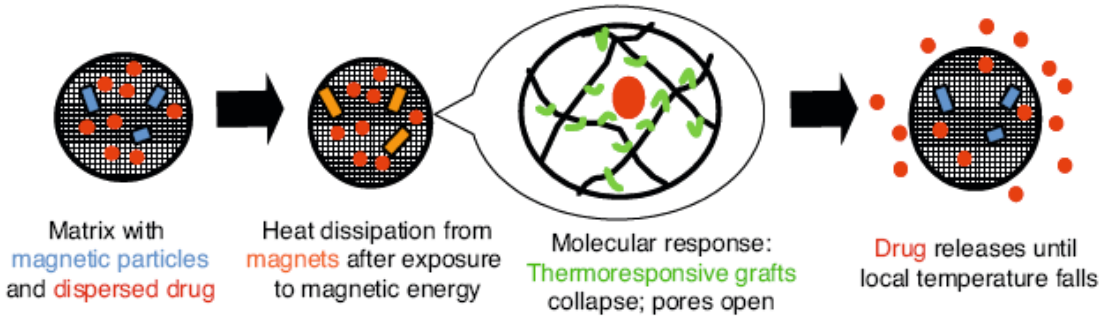

Figure 4. Depiction of magnetothermal responsive delivery system using a grafted hydrogel structure(*18*).

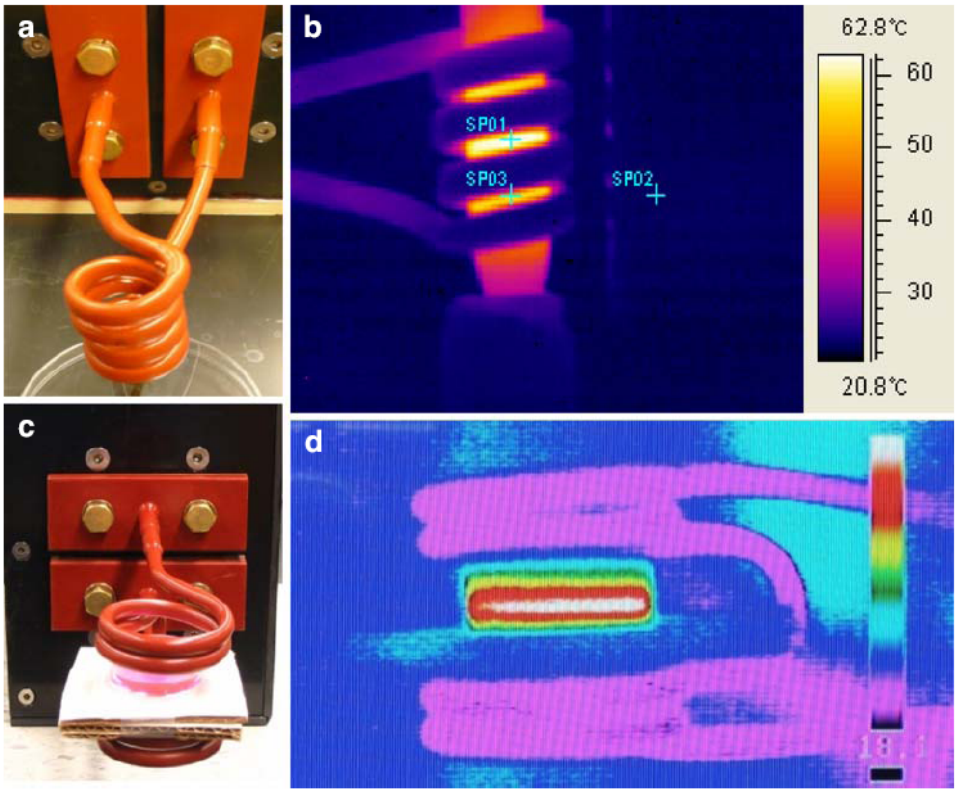

Figure 5. Magnetic coil for creating AC magnetic field and infrared temperature images of nanoparticle solutions (*18*)

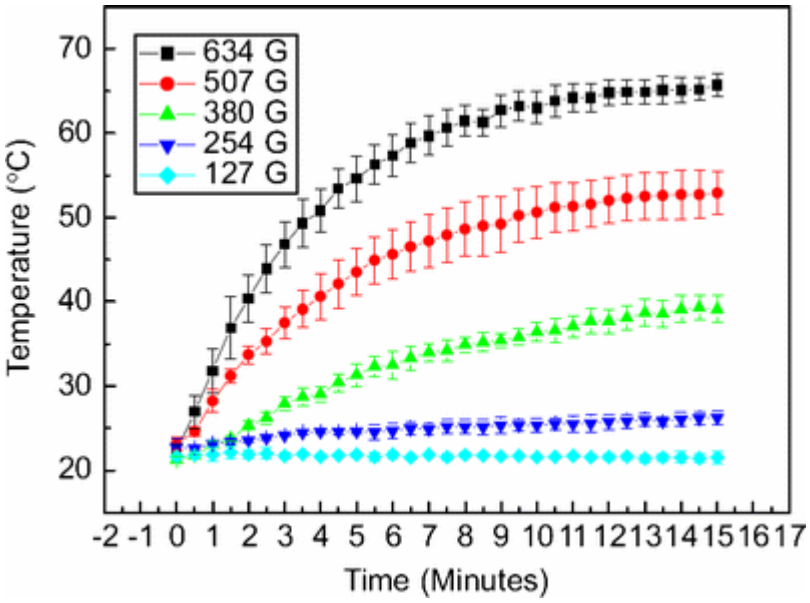

Figure 6. Effect of magnetic field intensity on heating profiles for cobalt ferrite nanoparticles exposed to 266 kHz AC field (*18*)

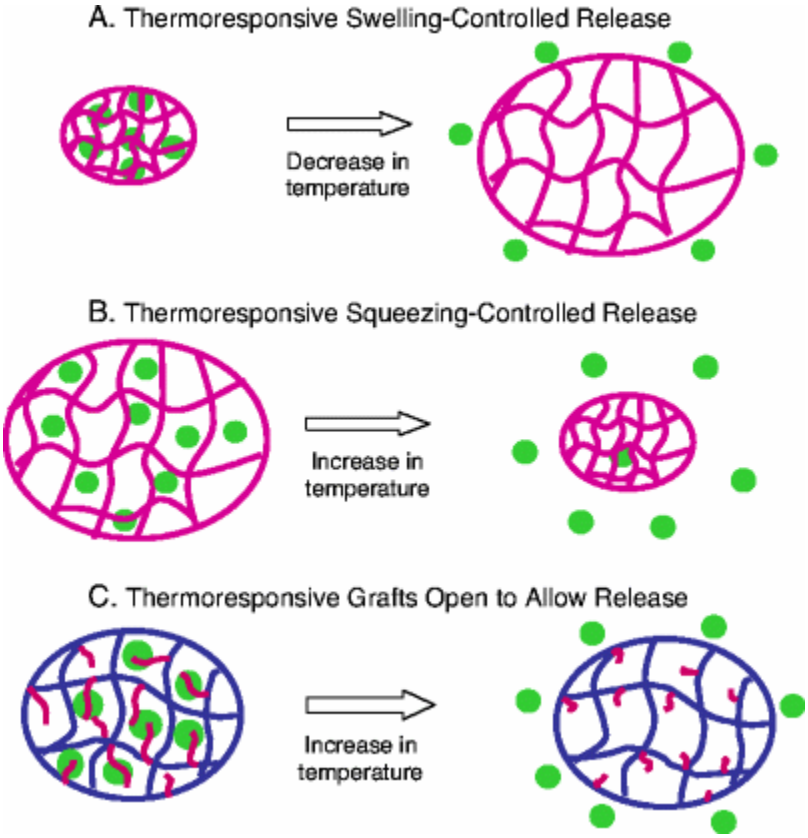

Figure 7. Thermoresponsive structures for controlled release. Squeezing-controlled and grafted systems can be triggered by magnetic heating (*18*).

Table 3. Types of Magnetic Nanoparticles Studied for Hyperthermia (*18*)

Magnetite Fe_3O_4 (73)
Maghemite, γ-Fe_2O_3 (73)
Hematite, Fe_2O_3 (74)
Cobalt ferrite, $CoFe_2O_4$ (75)
Manganese ferrite, $MnFe_2O_4$ (73,76)
Copper nickel, CuNi (77)
Iron platinum, Fe_xPt_y ($L1_0$ crystals) (78)
Cobalt, Co (hexagonal crystals) (73)
Iron palladium, FePd ($L1_0$ crystals) (79)
Cobalt platinum, CoPt (L10 crystals) (79)
Iron–cobalt, $Fe_{65}Co_{35}$ (80)

1.4. Magnetic Nanoparticles for nanomedicine

Nanoparticles whose dimensions range from one to hundreds of nanometers have been attracted and developed due to the ability to not only create a plethora of nanometer scale materials, but also to precisely tailor their properties for many novel and exciting applications. The nanomedicine is a quite interest field as the branch of medicine concerns with the application of nanotechnology to the prevention and treatment of disease. It involves the monitoring, repair, construction, and control of human biological systems at the molecular level, using engineered nanodevices and nanostructure.

Iron oxide is one of the most commonly employed materials for nanoparticle synthesis, having long history of biomedical applications (*32*). Iron oxide magnetic nanoparticles are smaller than approximately 20-30 nm in size containing a single magnetic domain with a single magnetic moment exhibiting superparamagnetism (*33*). Their relatively small size provides greater surface area-to-volume ratios which improve their binding kinetics and biodistribution for *in vitro* assay and *in vivo* imaging, respectively. Applying external magnetic field causes the alignment of magnetic moment of the entire particles yielding a fixed magnetization direction which gives imaging application such as magnetic relaxation switching (MRS) (Figure 8).

Iron oxide nanoparticles have a key advantage which is their natural integration into tissue physiology compared to other heavy metal-based nanoparticles. Iron and its oxides are metabolized, stored and transported through human tissues by proteins including ferritin, transferritin, hemosiderin, and others resulting in that iron is incorporated into the iron pool (*32*). Administration of 100 mg Fe/kg in rodent models

elicited no identifiable side effects, and dose increase to 600 mg Fe/kg did not induce subject death (*34*).

The common aqueous syntheses of superparamagnetic iron oxide nanoparticles (typically less than 20 nm) are alkaline coprecipitation and microemulsion-based precipitation/oxidation of ferrous and ferric salts (Fe^{+2} and Fe^{+3}). Nanoparticle size is controlled by solution ionic strength, pH values, and reactant stoichiometries (*35*). Another way to synthesize superparamagnetic iron oxide nanoparticles is the base-induced precipitation and oxidation of iron salt-surfactant complexes within the cores of nanoscale emulsions. This method is influenced by reactant stoichiometry, solvent systems, and surfactants-all of them give the significant influence of the complex dynamics of particle formation (*36*). Recently, Hyeon and coworkers reported a gram-quantity scale superparamagnetic iron oxide nanoparticle synthesis for formation of highly uniform and crystalline nanoparticles from inexpensive and nontoxic precursors by employing the microemulsion approach at elevated temperatures (*37*). They demonstrated a controlled nanoparticle size ranging from 2 to 10 nm using different precursor and surfactant ratios during the microemulsion procedure at 90 °C to promote the reaction. Figure 9 shows large-scale magnetic nanoparticle synthesis with 1-nm size control using iron pentacarbonyl precursors and oleic acid as the surfactant by Hyeon et al (*38*).

On synthesized iron oxide nanoparticles, selected hydrophobic surface ligands can be used as surfactants. For this purpose, the surface of nanoparticles needs to be modifided for biological applications in order to solubilize them in aqueous solutions. Generally, there are three routes for the surface modification from hydrophobic

nanoparticles as illustrated in Figure 10: (a) inorganic surface coating with teraethoxysilane produces an amorphous silica shell (*39*). (b) Polymer coating encapsulates the magnetic nanoparticles and native surface ligands (*40*). (c) The ligand exchange is to replace native surface ligands (*41*).

For the biological application of iron oxide nanoparticles, bioconjugation to additional biomolecule moieties such as targeting ligands (antibodies, aptamers, nucleic acid, etc.), labels (fluorescent dyes or radiolabels), and molecules (polyethylene glycol) can be utilized, which may also improve biocompatibility of magnetic nanoparticles. There are several bioconjugation approaches, for example, a passive adsorption, ligand-mediated linking, and covalent conjugation. Passive adsorption uses the electrostatic adsorption of highly charged biomolecules such as negatively charged nucleic acid onto positively charged polymer-coated nanoparticles. Ligand-mediated linking involves an adapter or binding protein and its appropriate ligand. For example, streptavidin-biotin protein-ligand pair has been employed to create magnetic nanoparticle-biomolecule conjugates (*42*). The most widely used covalent bioconjugation strategies are carbodiimide-mediated amide formation reaction, maleimide-thiol reaction, and orthpridyl disulfide-thiol coupling reaction.

Magnetic nanoparticles are utilized as sensitive negative contrast agents to accelerate the signal decay in a T2-weighted magnetic resonance (MR) image (*43*). The superparamagnetic iron oxide nanoparticle aggregation gives more efficiently dephasing the spins of surrounding water protons than disperse superparamagnetic nanoparticles, which results in providing a highly sensitive *in vitro* detection (*44*). This enhancement of the T2 signal has led to the development of magnetic relaxation switching (MRS)

technology for sensitive detection of oligonucleotides, proteins, enzymes, chiral compounds, carbohydrates, and viruses. Figure 11 shows the magnetic relaxation switching (MRS) technology: (a) schematic illustration of the transition of dispersed magnetic nanoparticles to nanoclusters with enhanced T2 relaxivity in the presence of ligands such as oligonucleotides. The linker- or ligand-mediated aggregation of nanoclusters can be enzymatically cleaved to yield disperse nanoparticles. (b) Atomic force microscopy (AFM) image of discrete magnetic nanoparticles. (c) Atomic force microscopy (AFM) image of nanoclustered magnetic nanoparticles in the presence of target molecule. (d) Nucleic acid detection with magnetic relaxation switching (MRS). A T2-weighted color-coded magnetic resonance (MR) image of wells of a 384-well plate. Each well contains similar amounts of probes. Each well contains similar amounts of probes. The concentration of matching and mis-matching target sequence is varied. (e) Decrease in T2 as a function of target sequence concentration, demonstrating detection sensitivity as low as 500 attomoles (*45*).

The field of *in vivo* molecular imaging needs improved magnetic relaxivities which increase magnetic resonance (MR) contrast sensitivity and controlled hydrodynamic size which increases uniform biodistribution profiles. For example, highly uniform $MnFe_2O_4$ nanoparticles conjugated to anti-Her-2 receptor antibodies were developed for *in vivo* magnetic resonance (MR) detection of cancer by Cheon et al (Figure 12) (*46*). Figure 12 (a) shows color maps of T2-weighted magnetic resonance (MR) images of a mouse implanted with the cancer cell line NIH3T6.7 at different time points after injection of $MnFe_2O_4$-Herceptin conjugates or CLIO-Herceptin conjugates. $MnFe_2O_4$-Herceptin conjugates perform gradual color changes at the tumor site, from red

to blue, indicating progressive targeting by those conjugates. In contrast, almost no change was seen in the mousetreated with CLIO-Herceptin conjugates. Figure 12 (b) presents T2*-weighted *in vivo* magnetic resonance (MR) images of NIH3T6.7 cancer cells implanted in mouse model imaged at 9.4 T. Top panel: Tumor area is circled with white dotted lines, and red dotted lines indicate the hypointense contrast provided by iron oxide nanoparticles. Bottom panel: color-coded magnetic resonance (MR) images to further delineate magnetic resonance (MR) signal changes. The temporal changes in the color maps indicate progressive diffusion and targeting events of the probes (low T2* signal) (*47*).

The *in vitro* ultrasensitive detection bioassays have been developed for target enrichment (target isolation) from complex biological specimens using magnetic separation with magnetic nanoparticles following multiplexed optical readout for detection at low concentrations. Figure 13 shows ultrasensitive detection schemes for assays developed by Mirkin and Groves: (a) fluorophore-based bio-barcode amplification assay to detect proteins developed by Mirkin (*48*). (b) Colorimetric bio-barcode amplification assay to detect cytokines developed by Groves (*49*). Both assays employ the magnetic nanoparticle-loaded microbeads for the separation of positive binding events from the false-positive background in order to increase signal-to-noise ratio. The high sensitivity of these assays is attributed to the high copy-number of dye-labeled DNA and strong optical properties associated with gold nanoparticles, respectively.

Magnetic nanoparticles with both imaging and therapeutic agents called multifunctional smart delivery system have received much attention for drug delivery

systems. Usually, such a system provides imaging functionality, cell-specific targeting, and controlled drug release (*50*). The advantages of magnetic nanoparticle-based drug delivery system are magnetic resonance imaging (MRI) contrast enhancement as well as the ability of guided localization of drug delivery by a magnetic field gradient (*51, 52*). Hyeon and coworkers recently designed and synthesized a multifunctional PLGA nanostructure incorporating 15-nm monodisperse superparamagnetic iron oxide (SPIO) for magnetic resonance (MR) imaging, 3-nm quantumdot (QD) for fluorescence visualization, and doxorubicin (DOXO) as a therapeutic agent (*53*). Figure 14 shows the fluorescence increase by confocal microscopy indicates the increase in multifunctional nanoparticle uptake mediated by the folate ligand and further uptake enhancement by the presence of an external magnetic field.

The highly efficient delivery of nucleic acid cargo such as anti-sense oligonucleotides, siRNA (small interfering RNA), and plasmid DNA (pDNA) has been also important in molecular biology, gene therapy, and clinical arenas. Figure 15 shows the example of in vivo optical imaging and effects on gene silencing in tumor with superparamagnetic iron oxide (SPIO)-siGFP constructs (*54*).

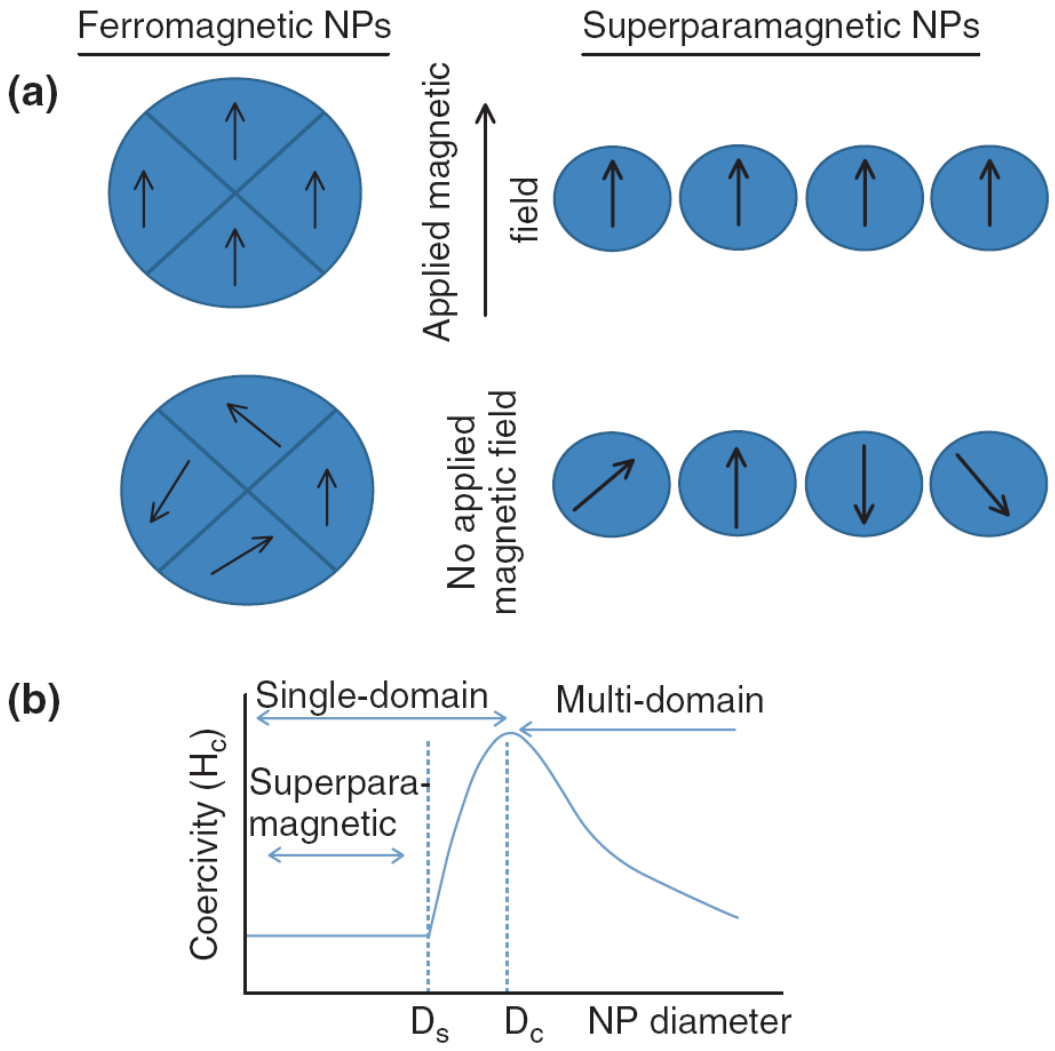

Figure 8. Magnetization behavior of ferromagnetic and superparamagnetic nanoparticles under an external magnetic field (D_s and D_c are the superparamagnetism and critical size thresholds.) (*32*).

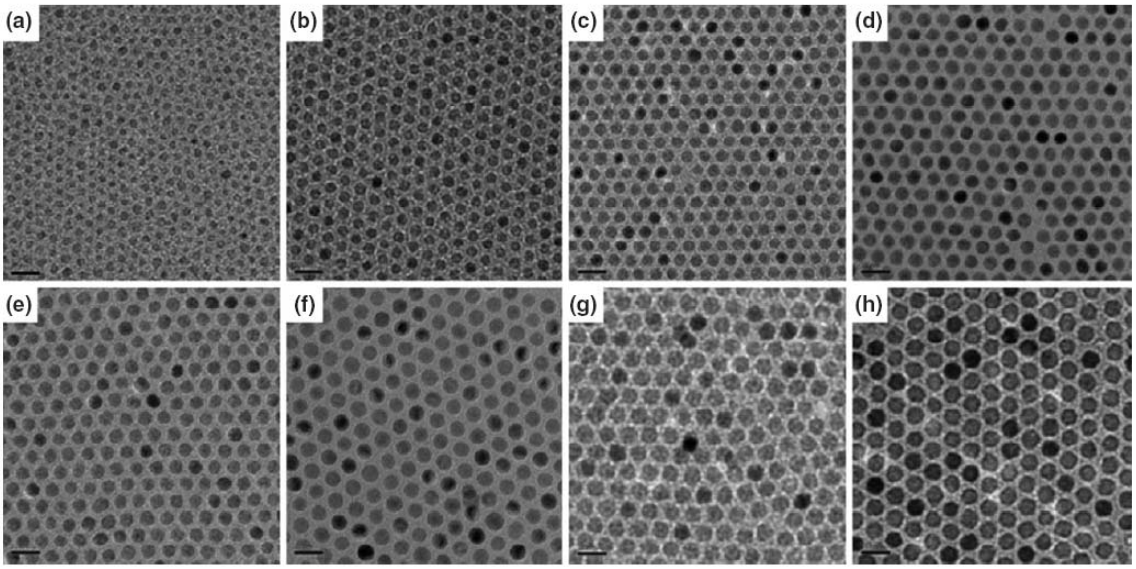

Figure 9. TEM micrographs of iron oxide nanoparticles with diameters of (a) 6 nm, (b) 7 nm, (c) 8 nm, (d) 9 nm, (e) 10 nm, (f) 11 nm, (g) 12 nm, (h) 13 nm (*38*).

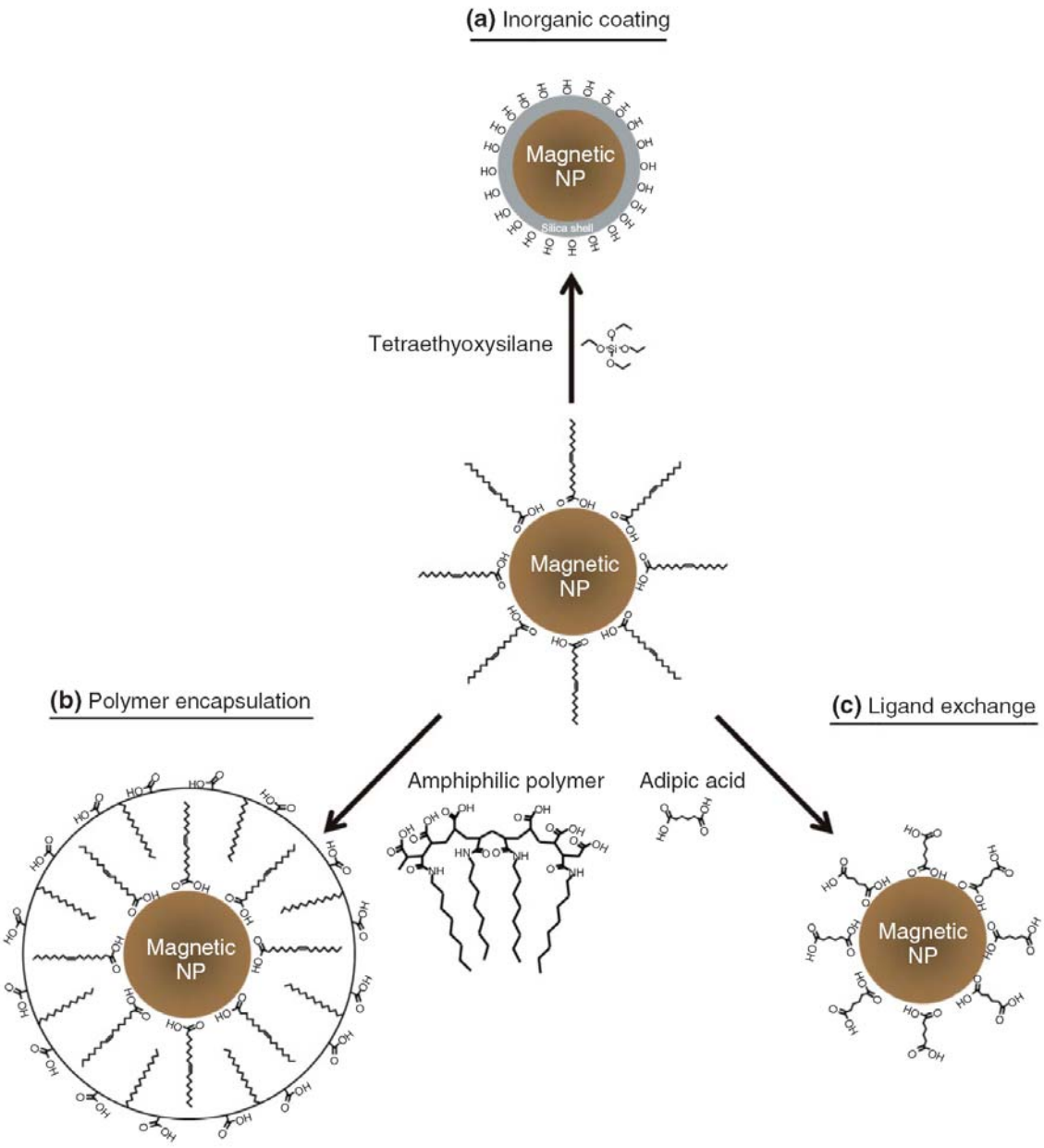

Figure 10. General surface modification schemes of magnetic nanoparticles (*32*).

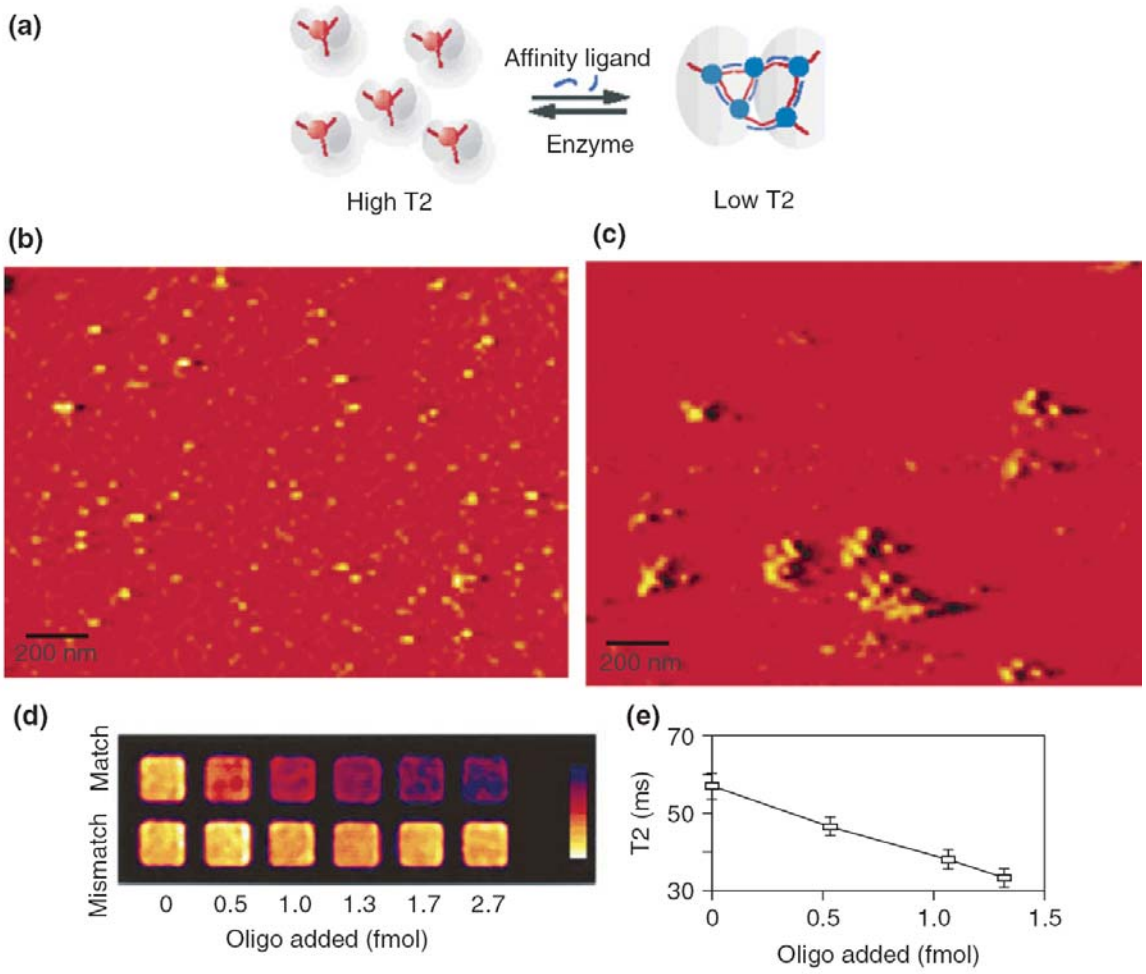

Figure 11. Magnetic relaxation switching technology (*45*).

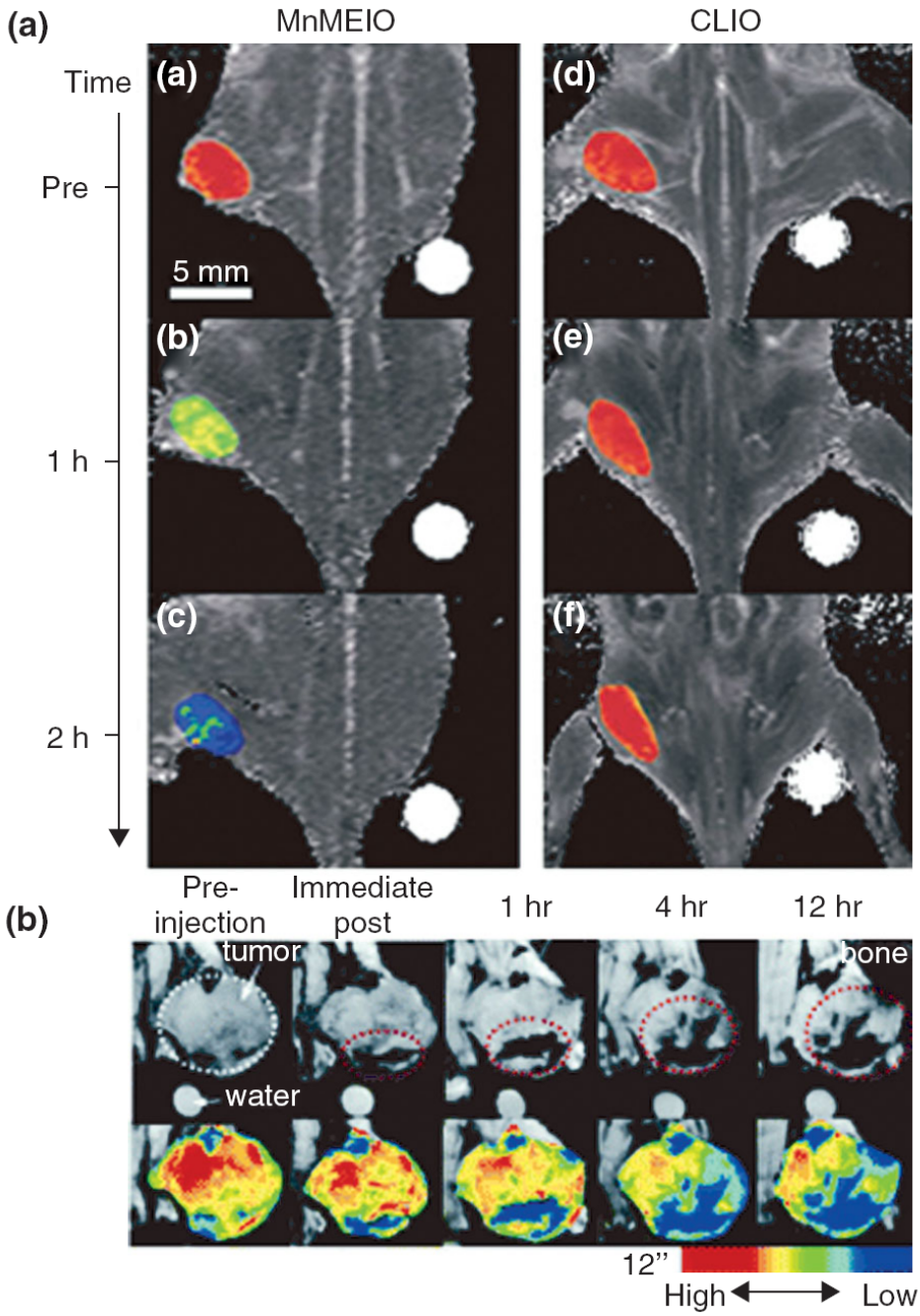

Figure 12. *In vivo* MR detection of cancer using magnetic nanoparticle-Herceptin bioconjugates (*46*, *47*).

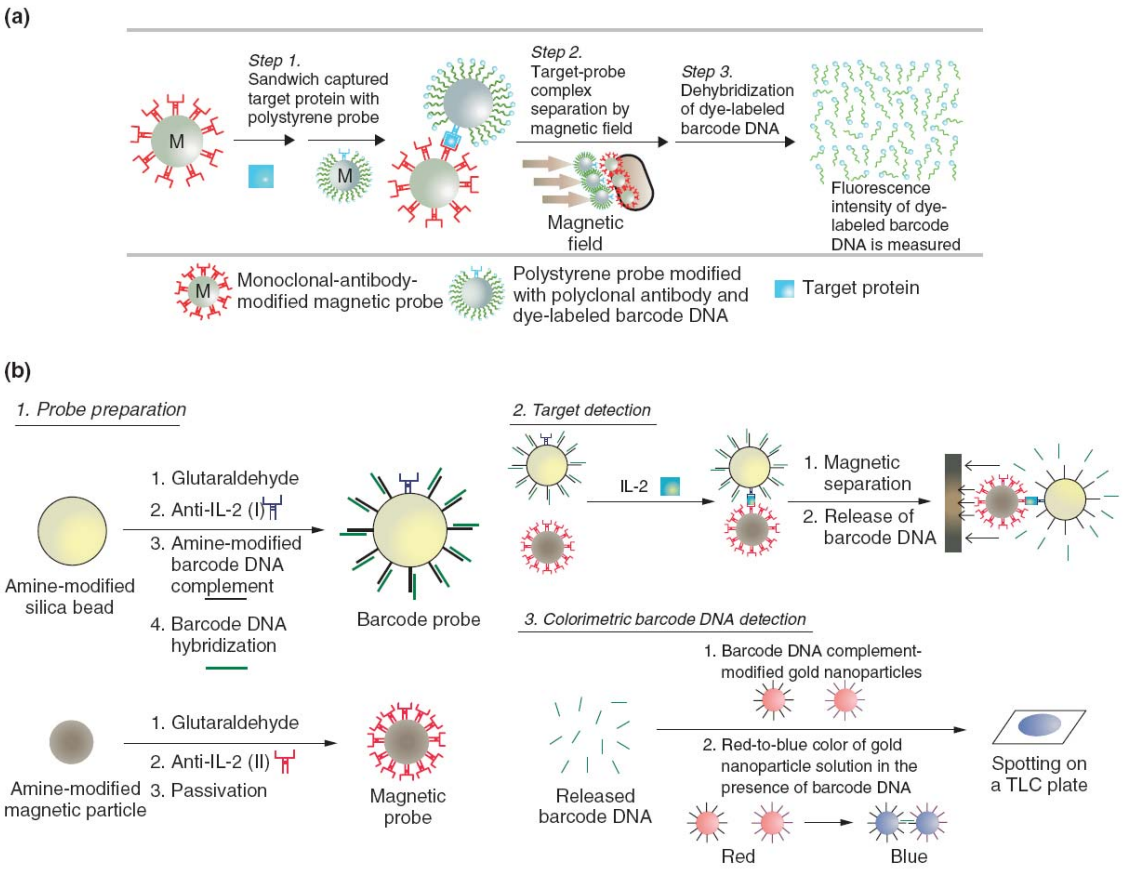

Figure 13. Ultrasensitive detection schemes for assays developed by Mirkin and Groves (*48*, *49*).

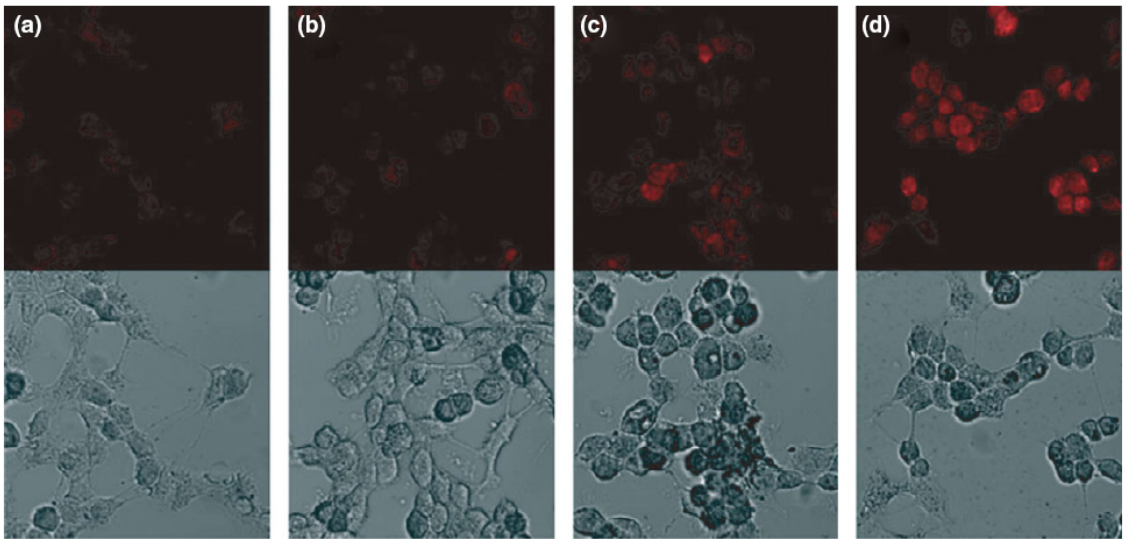

Figure 14. Confocal laser scanning microscopy of doxorubicin (DOXO) fluorescence and optical images of multifunctional PLGA nanoparticles developed by Hyeon et al. in KB cells treated with: (a) naked PLGA(superparamagnetic iron oxide (SPIO)/DOXO), (b) PLGA(SPIO/DOXO)-PEG, (c) PLGA(SPIO/DOXO)-Folate Nanoparticles and (d) PLGA(SPIO/DOXO)-Folate Nanoparticles exposed to an external magnetic field (*53*).

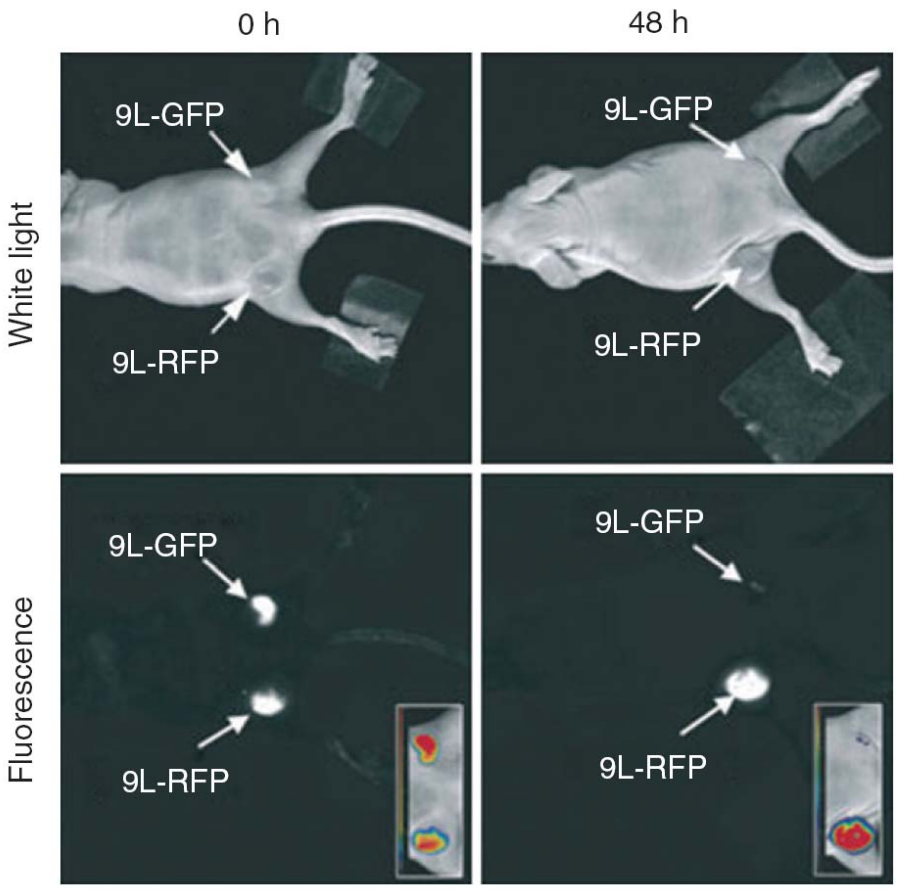

Figure 15. In vivo near-infrared optical imaging of SPIO-siGFP constructs and effects on gene silencing in tumors. Mice with bilateral 9L-GFP and 9L-RFP tumors are imaged before and 48 h after intravenous probe injection. Substantial decrease in 9L-GFP-associated fluorescence was observed, in contrast to 9L-RFP (no change). GFP and RFP images were acquired individually and later merged (*54*).

1.5. Ordered Mesoporous Materials in the Context of Drug Delivery System

The development of nanotechnology has provided the opportunity to investigate materials and their structure at the nanoscale range resulting in a new field of research and potential application. In 1991, Mobil Oil Corporation synthesized the silica-based MCM-41 (highly ordered mesoporous materials) which is characterized by their large surface area, pore volume, and pore size. These materials have been proposed not only for the field of catalysts, lasers, sensors, and solar cells, but also for the application of biomaterials (*55, 56*). Due to the outstanding features of surface and porosity, ordered mesoporous materials have shown to be excellent candidates for local drug delivery systems (*57*) and bone tissue regeneration. Silica-based mesoporous materials have also the remarkable character which is the easy surface functionalization for various purposes such as drug control release, labeling fluorescent marker, and targeting ligands.

These mesoporous materials are designed with adequate size pores which can host the molecules of drugs. The dimensions of the drug molecules are in the range of one nanometer (Figure 16). Therefore, any porous material with a pore diameter larger than one nanometer can easily take these therapeutic molecules into material matrix. Figure 17 presents that the pore size must affect the amount of drug readily adsorbed. With different pore diameters (2.5, 1.9, 1.6, 1.5 nm), the adsorbed amount of ibuprofen depends on the matrix pore size, and the release rate of ibuprofen from materials with different pore sizes is directly proportional to the pore size (Figure 17) (*58*). The matrix with well-odered pores clearly shows the homogeneity of the adsorption and release stage (*57*).

The pore walls in matrix can be functionalized with a wide range of chemical species resulting in modifying their adsorption properties. These features can make materials suitable to host different pharmaceutical species and to release drugs in a sustained regime for long time periods under appropriate conditions. Figure 18 shows the silanol groups (-OH) in the pore wall can facilitate certain interaction with carboxylic acid groups (-COOH) of ibuprofen molecules. These interactions can be chemically modified, through the adequate functionalization of the matrix walls; a precise functionalization performed on the pore walls could enable the control of the adsorption and release rates of a given drug (Figure 19) (*59*).

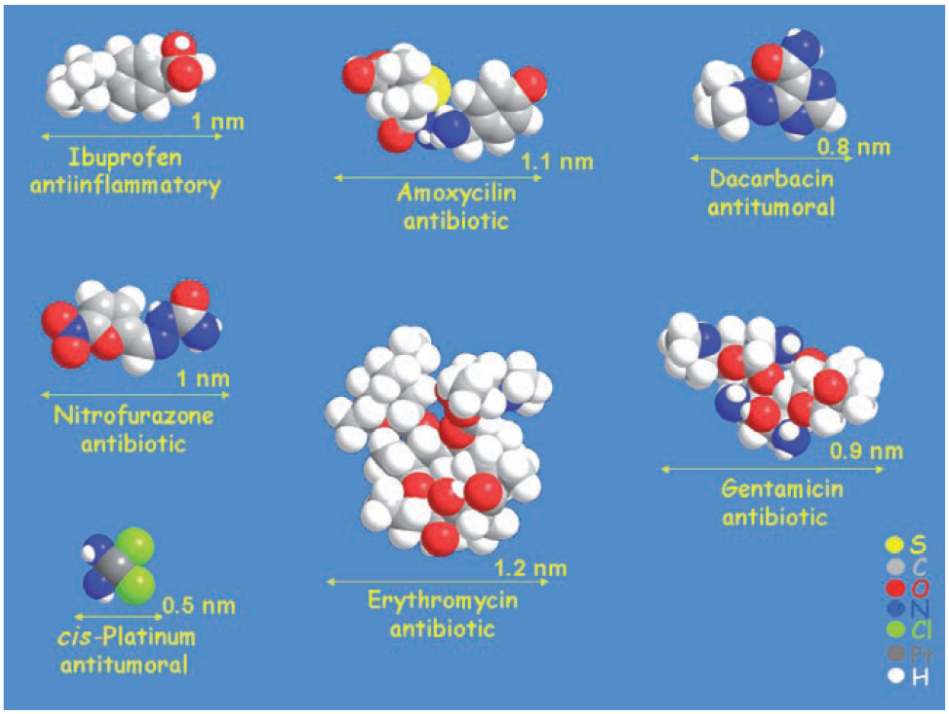

Figure 16. Molecules of several drugs with their sizes (*60*).

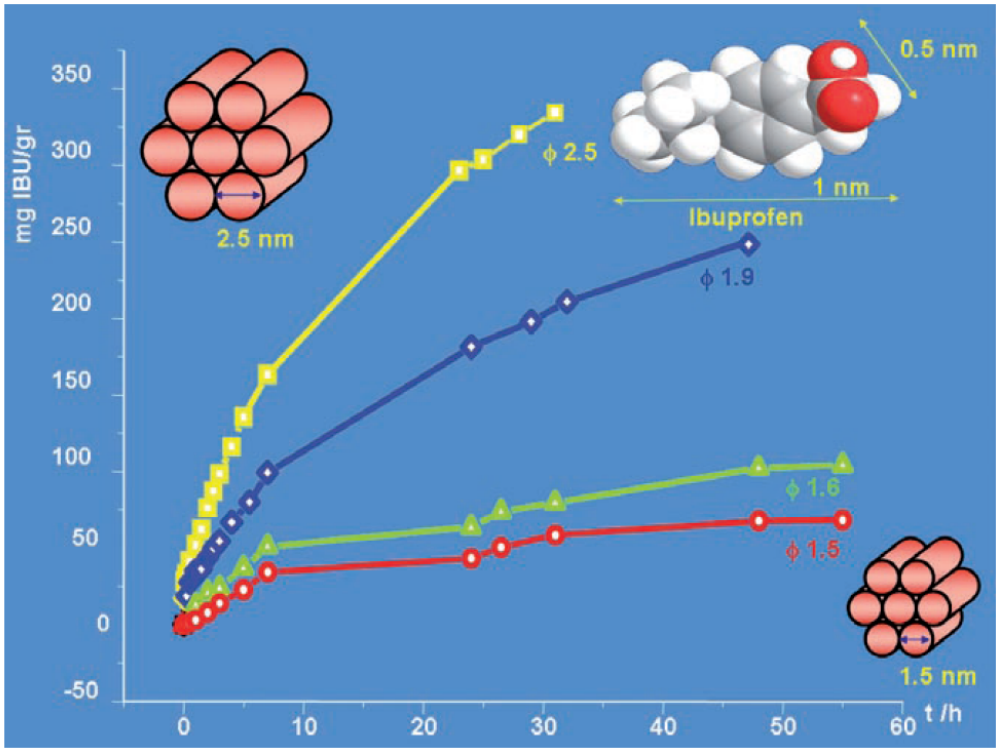

Figure 17. Release patterns of adsorbed ibuprofen in MCM-41 matrices with four different pore sizes (*58*).

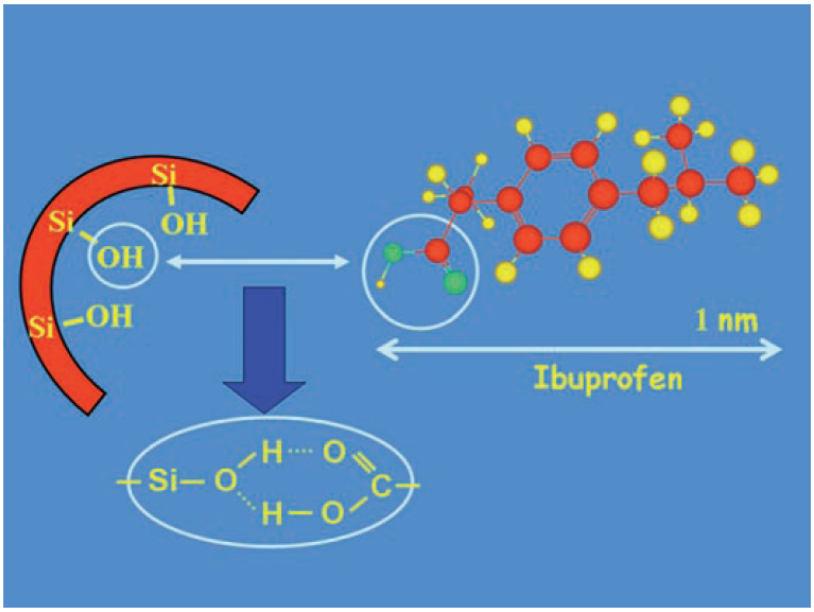

Figure 18. Interaction of OH group in the silanol at the pore wall of silica mesoporous material with the COOH group in the ibuprofen molecule (*60*).

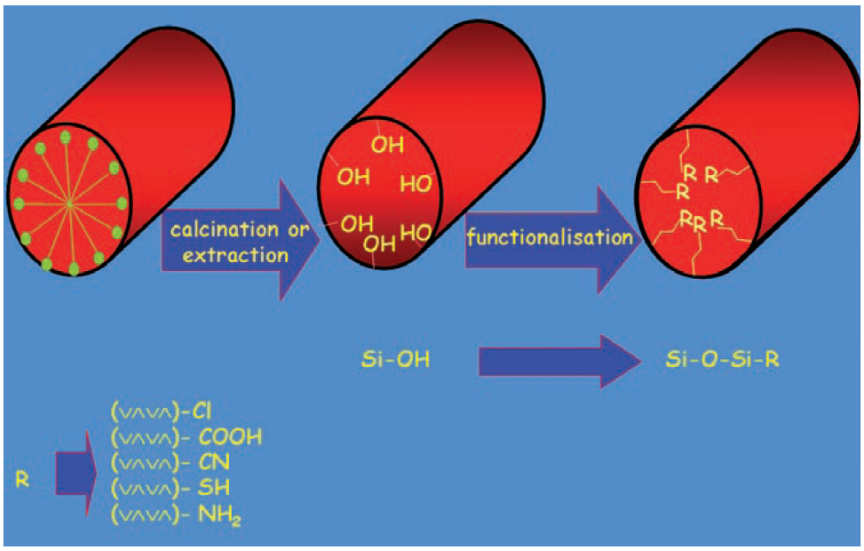

Figure 19. Simplified scheme of the pore wall functionalisation in a silica mesoporous material (*60*).

Chapter 2.

Creation of Remotely Controllable, On-Off Switchable Drug Release Methodology

2.1. Introduction

Current drug delivery systems with constant-rate, zero-order release are inadequate to meet the cyclic or irregular drug requirement in human body. Moreover, systemic and non-targeted drug delivery requires a higher dose with potentially multi-organ side-effects. There is a great need and a challenge to create new regimes of on-demand, drug release techniques with novel targeting strategies.

Biomedical use of nanotechnology, which led to the emergence of a new area called "nanomedicine", is an exciting and rapidly advancing field with potentially significant impacts on diagnosis and therapeutics for treatment of human diseases (*61-65*). Controlled drug release from nanoparticle drug carriers by external stimuli such as temperature, electric or magnetic fields, light radiation, and changes in pH (*66-73*) has attracted much attention for its potential in regulating and maintaining drug delivery of a desired therapeutic concentration range at a disease site. Localized, controlled drug

release improves the efficacy of the delivered drugs and minimizes toxic side effects (*74, 75*).

However, the much needed on-off switchable release using remote, external activation and subsequent de-activation on-demand at any given moment has not been fully addressed. A temperature dependent release, for example, based on a poly(*N*-isopropylacrylamide) hydrogel (*76*) is often based on more or less a one time release dosage due to swelling or deswelling of polymers when the drug carriers reach body temperature. Microelectromechanical Systems (MEMS) or poly(*N*-isopropylacrylamide) gel membrane-based drug release represent some examples of the pioneering techniques for on-demand release of drugs (*71-73*). However, the reversibility of on-off drug release and targeted delivery aspects, as well as penetration of tumors are often lacking in these devices. Hence, an alternative technique of switchable drug release based on smaller, maneuverable drug-cargo systems that can be placed in the desired drug delivery location is needed for targetable drug delivery therapeutics.

Hollow spheres have received much attention in recent years for a variety of technical applications including potential controlled-release, drug vehicles (*77-80*). Some of the hollow nanospheres (~50 – 150 nm diameter) have porous shells. This can be applied for passive drug delivery. However, there is no convenient, known way of triggered drug release from such nanospheres. In this thesis work, triggerable nanocapsules which contain magnetic nanoparticles responsive to external radio frequency (RF) magnetic field have been successfully created. This is in contrast to the regular hollow nanospheres for slow passive release of drugs. The new nanocapsule

material consists of bio-inert, bio-compatible or bio-degradable material that we can be selected from a variety of materials depending on specific medical applications.

2.2. Results & Discussion

Silica coated magnetic nanoparticles of Fe_3O_4 embedded in a polymer sphere matrix were fabricated by multi-step synthesis (*81*). We have substantially improved the process by first incorporating ~10 nm Fe_3O_4 nanoparticles (Fig. 20) into a polystyrene sphere which is then encapsulated in a silica shell, followed by dissolving away or burning away the polymer material present within the capsule, thus creating a hollow capsule configuration yet with magnetic nanoparticles trapped within. The shell material of the hollow capsules was constructed with a known biocompatible material, silica (SiO_2). The geometry of the capsule shells and porosity of the silica (SiO_2) wall was adjusted to be minimally permeable to the loaded drug-carrying solutions in the absence of the external stimuli of the applied magnetic field, but is suitably permeable to allow significantly enhanced drug release rates when activated by remote magnetic field. The novelty to our silica-coated magnetic nanocapsule (SiMNC) system lies within the interior of the capsules where the trapped Fe_3O_4 iron oxide nanoparticles (~10 nm diameter spheres) are present but with the polystyrene matrix material completely removed. We have obtained such a hollow nanocapsule structure by using a styrene-polystyrene (PS) emulsion approach combined with silica shell processing. The details of the capsule synthesis materials and methods are described in the methods section.

Shown in Figure 21 is a schematic illustration of the processes utilized for fabrication of such hollow silica magnetic nanocapsules (SiMNC) with trapped magnetic nanoparticles inside. The polystyrene (PS) polymer material inside the capsule was burnt out to create the hollow core capsule, by slowly heating to ~500^{o}C for 6 hr so that the

emptied capsule interior space can be later used for drug insertion (Fig. 21). An analysis by FT-IR proves that the polystyrene (PS) is completely burnt away by the heat treatment in air. In the FT-IR data, the C-H (aromatic) and the -CH_2- of the polystyrene (PS) stretching vibrations occur at 3000-2800 cm^{-1} and the C-H bending vibration peak is shown between 1480 and 1400 cm^{-1} (*82*). These peaks present in the polystyrene-containing nanocapsules disappear completely after our heat treatment. The removal of polystyrene polymer is apparent in the magnified FT-IR data shown Fig. 22. The TEM micrograph shown in Fig. 23 represents the resultant silica coated core/shell spheres with a high density of trapped magnetic particles. The diameter of the core space containing dense magnetic nanoparticles is ~60 - 100 nm in average diameter and the thickness of silica shell is 15~25 nm depending on the specifics of processing conditions. An alteration of the synthesis parameters can produce reduced overall diameter capsules of ~100 nm or smaller. The amount of Fe_3O_4 nanoparticles is estimated to be ~80 wt % (~45 volume %) within the hollow space inside the capsule (*81*).

Switchable on-off release of hydrophobic drug Camptothecin (Cpt), one of the anti-cancer drugs chosen for this study, from our hollow silica-coated magnetic nanocapsule (SiMNC) was controlled by applying radio frequency (RF) field. Camptothecin was loaded into the ~150 nm diameter hollow capsule vehicle using vacuum loading process and then remotely activated for drug release by applied radio frequency (RF) field (further details of the process is found in the methods section). Briefly, the camptothecine (Cpt) anti-cancer drug was dissolved first in DMSO (dimethyl sulfoxide) solvent, vacuum suctioned into the hollow capsules and then thoroughly washed with DI water. The camptothecine-containing nanocapsules were dispersed in water and subjected to a radio

frequency (RF) magnetic field. To measure the drug release amount, the silica-coated magnetic nanocapsules (SiMNCs) were removed by settling them down by a magnet for 2 minutes, and the drug content in the remaining solution was measured using UV/VIS absorption spectrophotometer. For actual therapeutic applications, appropriately programmed on-off magnetic field cycles may be utilized, for example, to enable controlled release over extended periods of time with suitably minimized toxic side effects, and also to minimize possible nanocapsule overheating damage. Therefore an on-off cyclic release experiments were conducted as follows.

Figure 24 shows the drug release data based on a hydrophobic anti-cancer drug, camptothecin (Cpt) using our silica-coated magnetic nanocapsule (SiMNC), with the measured amount of released drug plotted as a function of on-off switch cycle of applied radio frequency (RF) magnetic field (at 100 kHz). A dramatic change in the amount of released drug is evident when the remote magnetic field is switched “on” vs. “off”. Such drug release on-off cycles are repeated at least several cycles in the experiment. The hollow silica-coated magnetic nanocapsule (SiMNC) stores and releases much more amount (by a factor of at least ~x20) of camptothecine (Cpt) per mg of magnetic nanocapsules (NCs) as compared to the case of silica-coated magnetic nanocapsule (SiMNC) with the core still filled with polystyrene (PS) (before the burn-off of polystyrene) as is discussed later. The non-hollow nanocapsules obviously could not be loaded with camptothecine (Cpt) because the core was packed with polymer. (A small amount of drug release was noted from the latter, which is probably due to the surface adhesion of some drug molecules on the silica outer surface.) It is evident that the emptied capsule’s interior space can be used to load hydrophobic drugs more efficiently

compared with the polystyrene (PS) core-filled capsule. Uniquely, we have also designed our system so that while the hollow core can carry and release hydrophobic drugs, the interior of the silica shell and the outer silica shell surface possess hydrophilic characteristics, which will naturally resist the leakage of hydrophobic drug based on opposing surface properties once the drug is loaded. Therefore the trapped hydrophobic drugs in the interior of silica-coated magnetic nanocapsules (SiMNCs) are not permitted to be easily diffused out of the nanocapsule without additional stimuli to overcome the hydrophilic shell surface repulsion. A similar on-off switchable drug release behavior was also observed for the hydrophilic type anti-cancer drugs such as Doxorubicin, with the data shown in Fig. 25. Doxorubicin was loaded into the hollow nanocapsules by vacuum suction, with the loaded capsules washed by deionized water and centrifuged. The degree of remotely activated drug release was measured by UV/VIS spectrophotometer.

Possible release mechanism for the observed on-off switchable drug release most likely involves the heating of magnetic nanoparticles trapped within the nanocapsules. The remote high-frequency radio frequency (RF) magnetic field, at the frequency used (100 KHz) selectively heats the magnetic nanoparticles in the hollow shell interior to induce a temperature gradient and stimulate accelerated drug release.

It is hypothesized that the remotely applied magnetic field primarily induces magnetic particle heating and causes the localized liquid temperature inside the nanosphere to rise, as illustrated in Fig. 26 upper diagram. This mechanism is in agreement with the well established magnetic nanoparticle heating in the case of magnetic hyperthermia treatment of cancer cells. The magnitude of temperature rise will

be dependent on materials and operational parameters such as the concentration and types of magnetic particles, radio frequency (RF) and intensity of applied field, and duration of field. The rate of diffusion during the "on" demand of drug release is controllable by the degree and duration of magnetic heating as well as the predetermined nanoporosity of the shell material, silica. For a demonstration of remote heating as a function of applied field duration, we carried out such radio frequency (RF) heating experiments using Fe_3O_4 magnetic nanoparticles with a lower concentration than in our silica-coated magnetic nanocapsules (SiMNCs). The magnetic nanoparticles (~10 nm average diameter) in a water base solution were heated using the same 100 kHz radio frequency (RF) field as we used for drug release from the nanocapsules, the results of which showed a time-dependent gradual temperature rise (Fig. 27) as measured by a optical fiber temperature sensor. A similar temperature rise is anticipated when the magnetic particles are inside the hollow sphere. The resultant temperature gradient between inside vs. outside of the sphere is a key element in inducing the diffusional delivery of the stored drug on-demand when the field is applied for a specific duration.

The drug release from our silica-coated magnetic nanocapsules (SiMNCs) may also be induced by utilizing other means. For example, remote low-frequency, direction-changing magnetic field may be utilized to induce magnetic particle movements and vibrations within the hollow shell and enable accelerated drug release. This is schematically illustrated in Fig. 26 lower diagram as compared to the nanoparticle heating approach described in the Fig. 26 upper diagram. The use of ultrasonic vibrations is also conceivable. These alternative remote activation approaches are beyond the scope of this report, and will be discussed in future publications.

In order to visualize the remotely radio frequency (RF) activated drug release phenomenon from our silica-coated magnetic nanocapsule (SiMNC) system, a fluorophore which gets excited in its energy state and then relaxes consequently emitting light, was utilized. This chemical release study (Fig. 30) demonstrates that the controlled release of a chemical compound can be activated by external radio frequency (RF) magnetic field to give rise to the observed color change. Experimental details are given in the methods section. Such a remote-activated color change by itself is an intriguing phenomenon which could possibly be exploited for some interesting visual displays, signaling devices, on-demand or on-off switchable activation of chemical reactions.

This Chapter, in full, has been submitted for publication, “Magnetically Vectored Nanocapsules for Tumor Penetraion and Remotely Switchable On-Demand Drug Release”, by Seong Deok Kong, Weizhou Zhang, Jun Hee Lee, Karla Brammer, Ratnesh Lal, Michael Karin, and Sungho Jin.

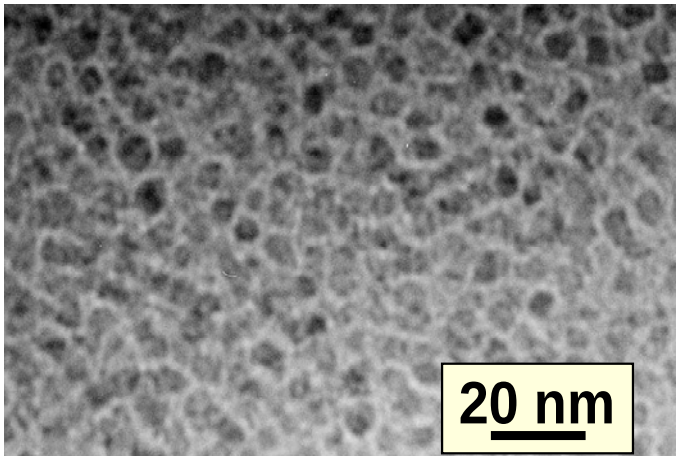

Figure 20. TEM image of ~10 nm diameter Fe_3O_4 iron oxide magnetic nanoparticles synthesized for inclusion in the nanocapsules.

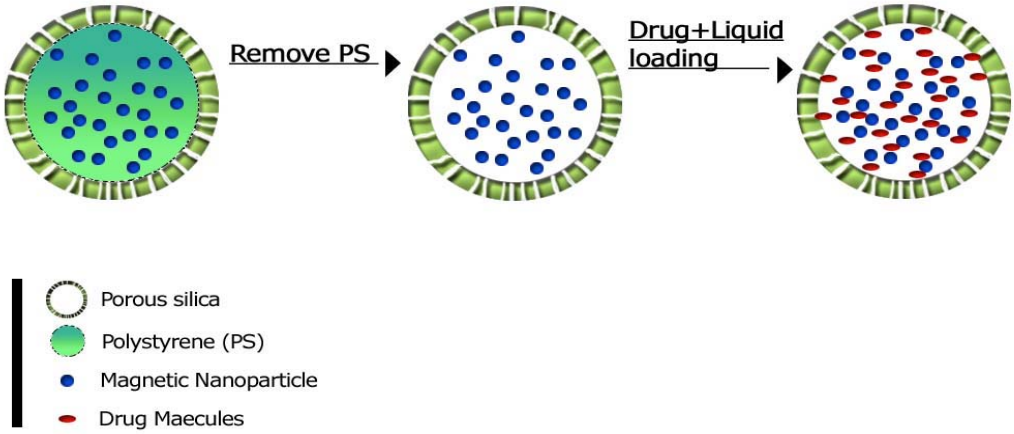

Figure 21. Schematic illustration showing the preparation steps of drug-containing hollow SiMNCs with high saturation magnetization.

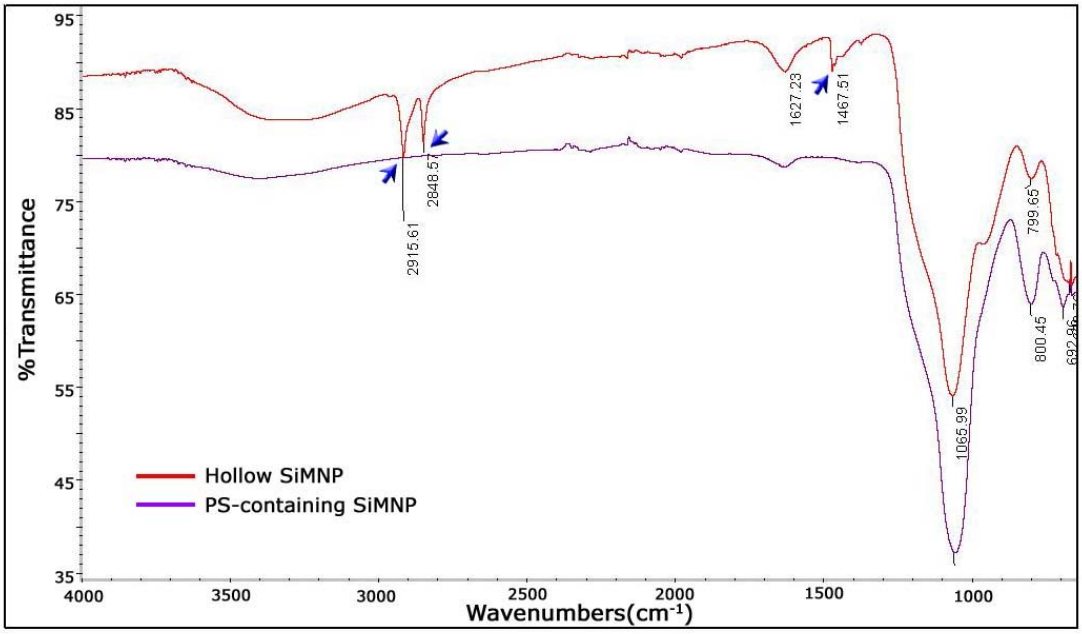

Figure 22. A portion of the FT-IR data showing the removal of polystyrene (PS) from inside the nanocapsules. PS material inside the capsule was burnt out to create the hollow core capsule so that the emptied capsule interior space can be later used for drug insertion as illustrated in Fig. 21. An analysis by FT-IR (Fourier Transform Infrared) spectroscopy proves that the PS is completely removed by the heat treatment. C-H (aromatic) and -CH_2- of the PS stretching vibrations occur at 3000-2800 cm^{-1} and the C-H bending vibration peak occurs between 1480 and 1400 cm^{-1} (*82*). These peaks present in the PS-containing nanocapsules disappear completely after heat treatment.

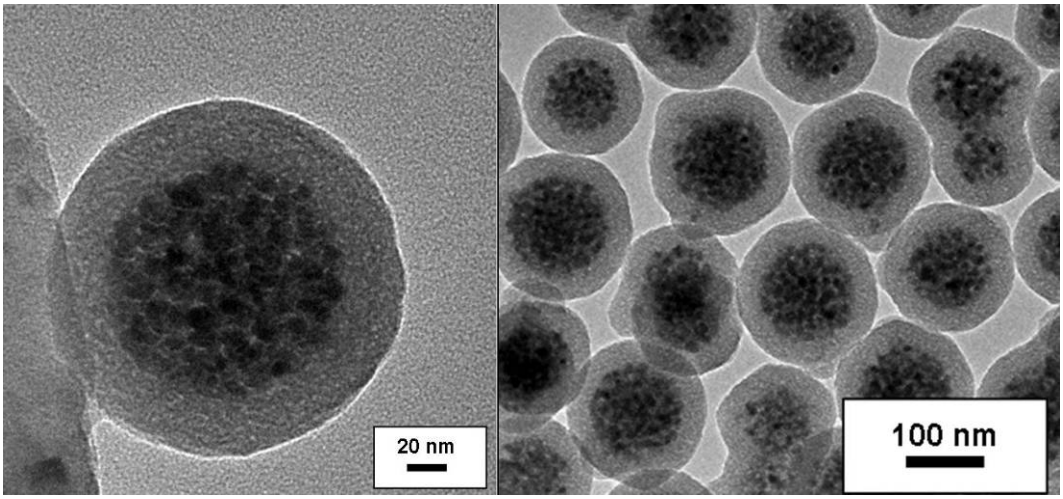

Figure 23. TEM micrograph showing high-density of trapped magnetic nanoparticles in SiMNCs. The average diameter of the core space containing dense magnetic nanoparticles is ~60 - 100 nm in average diameter and the silica shell is 15~25 nm thick. The amount of encapsulated Fe_3O_4 nanoparticles is estimated to be ~80 wt % (~45 volume %).(*81*)

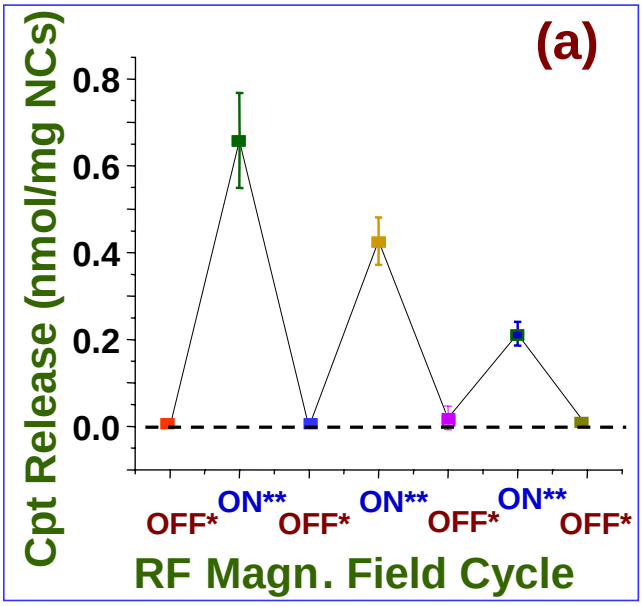

Figure 24. On-off switchable release from the SiMNC nanocapsules. (A) Release of hydrophobic camptothecin (nanomole per mg nanocapsule, NC) by RF magnetic field on-off cycling (switch-on period=10 seconds, switch off=5 minutes), The hollow SiMNC capsules store and release much more (by a factor of at least ~x20) Cpt per mg of magnetic nanocapsules as compared to the case of SiMNC with the core still filled with PS (before its burn-off) as the non-hollow nanocapsules obviously could not be loaded with much Cpt drug because the core was packed with polymer. (A small amount of drug release was noted from the latter, which is probably due to the surface adhesion of some drug molecules on the silica outer surface.) We have also designed our system such that while the hollow core can carry and release hydrophobic drugs, the interior of the silica shell and the outer silica shell surface possess hydrophilic characteristics, which will naturally resist the leakage of hydrophobic drugs based on opposing surface properties.

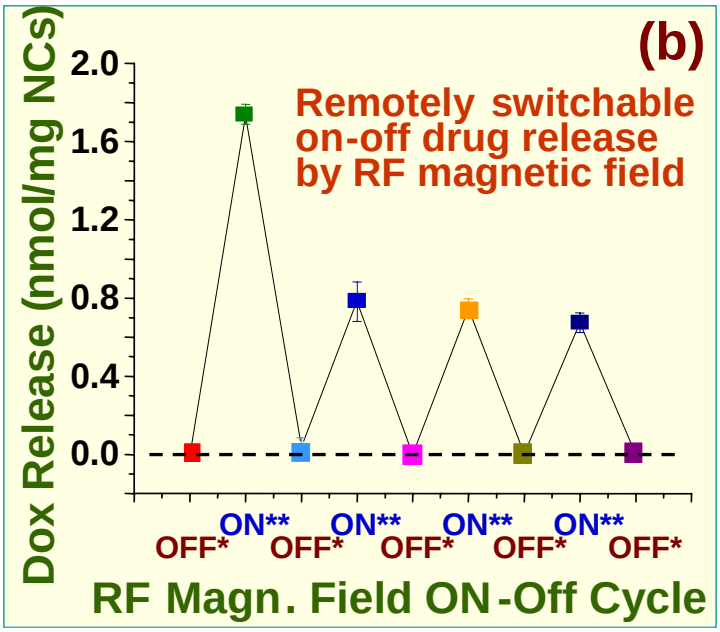

Figure 25. A similar switchable release is demonstrated for hydrophilic doxorubicin from the nanocapsules by RF field.

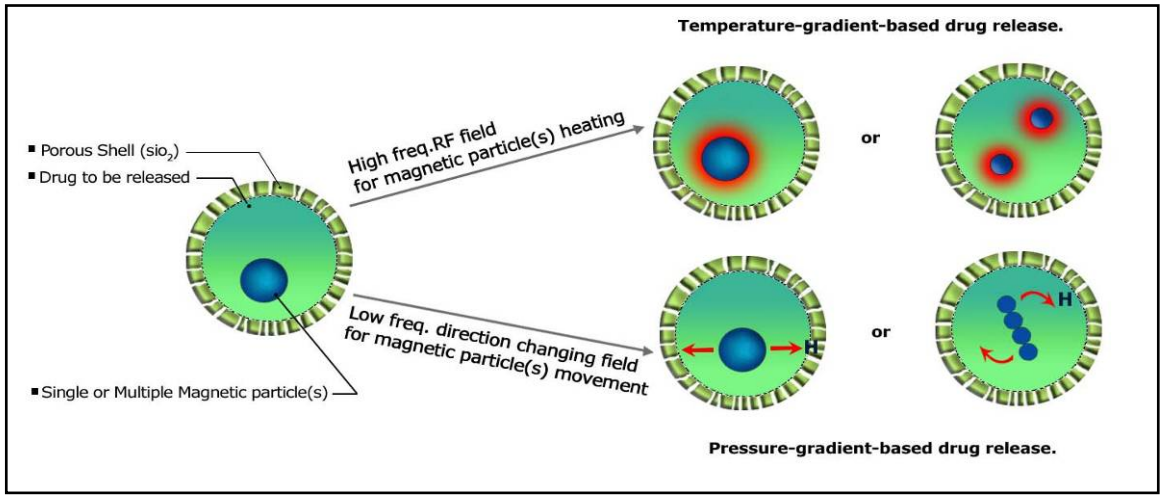

Figure 26. Controlled drug release from Camptothecin-containing SiMNCs by RF magnetic field on-off cycling. Schematic illustration of temperature-gradient-based or pressure-gradient-based drug release mechanism. The magnitude of temperature rise is dependent on materials and operational parameters such as the concentration and types of magnetic particles, RF frequency, intensity and duration. The drug release rate is controllable by the RF heating as well as the predetermined nanoporosity of the shell material, silica.

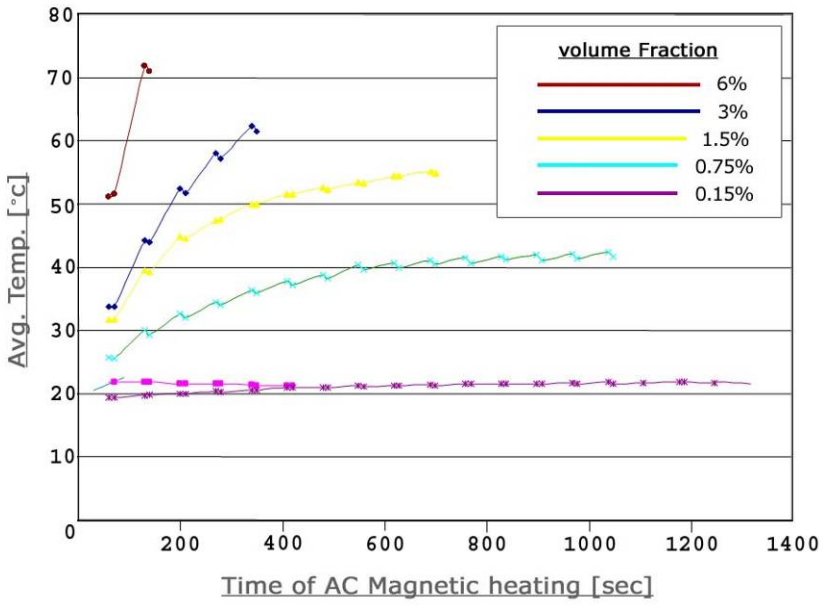

Figure 27. Remote magnetic field heating of fluid (water) containing magnetic nanoparticles. The data shows temperature rise vs. RF field duration for various amounts of 10 nm magnetic nanoparticles of Fe_3O_4. A similar temperature rise is anticipated when the magnetic particles are inside the hollow sphere.

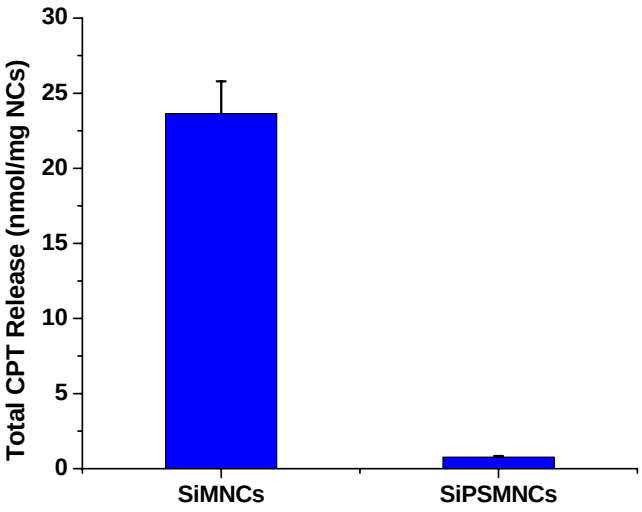

Figure 28. The comparison of total amounts of Camptothecin release from hollow SiMNCs vs. PS-containing, nonhollow SiMNCs.

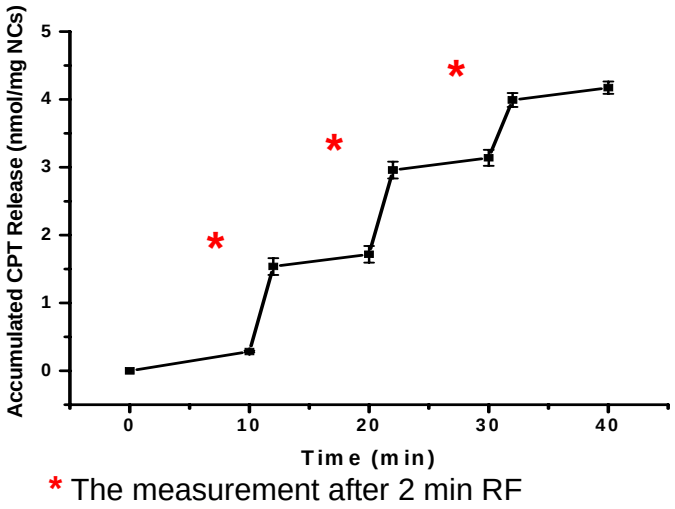

Figure 29. Cumulative amount of Camptothecin by longer period, repeated switchable release (switch-on period=2 minutes, switch-off period=8 minutes) shown up to 3 cycles.

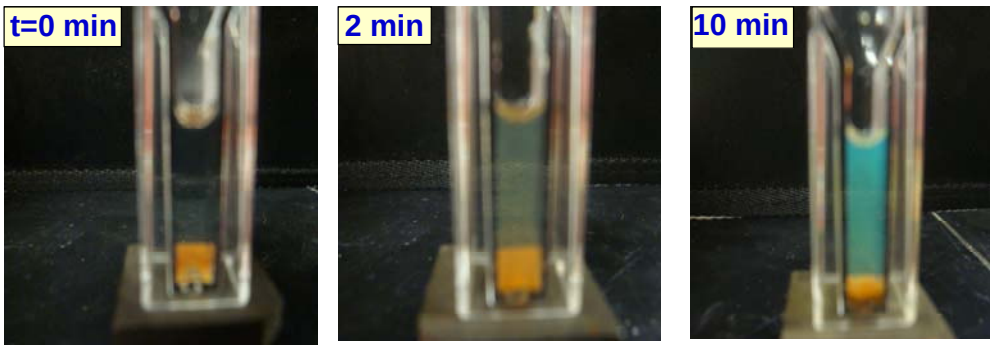

Figure 30. Visualization of remote RF controlled release of chemicals from the SiMNC containing. Such a remote-activated color change is an intriguing phenomenon by itself, which could possibly be exploited for visual displays, signaling devices, switchable activation of chemical reactions or catalytic/enzymatic/biological reactions.

2.3. Methods

2.3.1. General Comments

All reagents were purchased from Sigma-Aldrich, Inc. and Alfa Aesar, and used without further purification. The microscopy characterization of synthesized nanoparticles and magnetic nanocapsules were carried out using a transmission electron microscope (FEI Tecnai G2 Sphera with 200 kV accelerated voltage). Various chemical, magnetic and optical measurements were performed using FT-IR (Nicolet 6700 analytical MCT FT-IR Spectrometer), SQUID magnetometer (Quantum Design MPMS2) and UV/VIS spectrophotometer (Thermo BioMate3). For the generation of RF magnetic field, Lepel LSS-2.5 RF power supply equipped with a water cooled solenoid was used.

2.3.2. Synthesis of mono-disperse Fe_3O_4 nanoparticles

Polystyrene nanospheres with trapped magnetic nanoparticles (as a precursor component for synthesis of silica coated magnetic nanocapsules (SiMNC)) were prepared by combining mini-emusion/emulsion polymerization and the sol-gel technique according to Hong Xu *et al (81)*. Briefly, a mixture of 24g $FeCl_3 \cdot 6H_2O$ and 9.82g $FeCl_2 \cdot 4H_2O$ was reacted with 50 ml of ammonium hydroxide under nitrogen gas at 80 ^oC, and then the solution was allowed to react for 1.5 hours after the addition of 3.76 g of oleic acid. The magnetite nanoparticles (see TEM micrograph, Fig. 23) so fabricated were washed with deionized water until neutral pH and then were transferred *in situ* into octane.

2.3.3. Nanocapsule formation

Magnetite mini emulsion and styrene mini emulsion were prepared using ultrasound and microporous glass membrane (SPG membrane, SPG Technology Co., Ltd). With these emulsions, mono disperse Fe_3O_4/polystyrene nanospheres were synthesized with 40 mg potassium peroxydisulfate (KPS) at 80 ^oC for 20 h in nitrogen atmosphere. The synthesized Fe_3O_4/polystyrene nanospheres were centrifuged and then were redispersed into 10 ml 0.5wt. % polyoxyethylene sorbitan monolaurate aqueous solution with ultrasonic treatment to form a new suspension. The suspension was added into 20 ml 2-propanol, and then 0.5 ml ammonium hydroxide and 20 μl TEOS were consecutively added into the above reaction solution. The silica encapsulation reaction was performed at room temperature for 48h. The resultant silica magnetic nanospheres were collected and washed three times by ethanol and water, respectively.

2.3.4. FT-IR analysis for polystyrene removal

The complete FT-IR analysis data for polystyrene peaks before *vs* after the burn out treatment is shown in Fig. 22. In the FT-IR data, the C-H (aromatic) and the -CH_2- of the polystyrene (PS) stretching vibrations occur at 3000-2800 cm^{-1} and the C-H bending vibration peak is shown between 1480 and 1400 cm^{-1} (*82*). These peaks present in the PS-containing nanocapsules disappear completely after the heat treatment. The FT-IR analysis data proves that the polystyrene (PS) within the silica shell is completely burnt away by the heat treatment in air.

2.3.5. Preparation of Camptothecin (Cpt)-loaded SiMNCs

For fabrication of hollow SiMNCs, the polystyrene (PS) nanosphere material within the silica shell was burnt out at 400-500 ^{o}C for 3-6 hrs to generate the hollow SiMNCs. The magnetic nanoparticles do not burn out and remain trapped within the silica nanocapsule. Then a hydrophobic anticancer drug, Camptothecin (Cpt), dissolved in DMSO (dimethyl sulfoxide) and THF (tetrahydrofuran), was inserted into the partially hollow nanocapsule containing only Fe_3O_4 magnetic nanoparticles at room temperature by vacuum drug loading method. 1 mL solution (50 μL of DMSO + 950 μL of THF) containing 1 mg Cpt was loaded into 5 mg of SiMNCs. After drugs were loaded, the drug-containing capsules were washed by de-ionized (DI) water 3-5 times and centrifuged. And then the supernatant was removed completely. The washing process was repeated until the supernatant was clear. The particles were settled down using a permanent magnet and then the supernatant was removed. The particles were dried using a supercritical CO_2 drier. All process was performed in the fume hood with well ventilated facilities.

The Cpt-containing nanocapsules were dispersed in water and subjected to an RF magnetic field. To measure the amount of released drug by remotely RF activation, the SiMNCs were removed by settling them down by a magnet, and the drug content in the remaining solution was measured using UV/VIS absorption spectrophotometer. For actual therapeutic applications, appropriately programmed on-off magnetic field cycles may be utilized, for example, to enable controlled release over extended periods of time with suitably minimized toxic side effects, and also to minimize possible nanocapsule overheating damage. Therefore an on-off cyclic release experiments were conducted.

2.3.6. *In vitro* remote activated drug release measurement

After Cpt-loaded SiMNCs were prepared, the drug-containing capsules were washed by PBS twice and centrifuged. And then the supernatant was removed completely. When drug-loaded SiMNCs were prepared, the remote activated drug release was measured by UV/VIS spectrophotometer. For the first 10 min, the solution containing fresh 0.5 μL PBS was left without RF and then the Cpt release was measured after SiMNCs were settled down by magnet for 4 min. After the measured solution was replace to the fresh 0.5 μL PBS, the solution was exposed to RF (at 100 KHz) for 2 min. Then SiMNCs were settled down by magnet for 4 min. After the Cpt supernatants were cleared of floating particles, they were measured using UV/VIS absorption for drug contents dissolved in the solution. After the switch "ON" measurement is done, SiMNCs were suspended in the fresh 0.5 μL PBS again, and then the solution was left for 8 min without RF. Next, SiMNCs were settled down by magnet for 4 min after waiting for 8 min of "off" time, they were also measured by UV/VIS spectrophotometer. The switch "ON-OFF" measurements were taken alternately and the release profile was graphed.

2.3.7. Visualization experiments for remote activation and release of fluorescent chemicals from remote activated magnetic capsules (hollow SiMNCs)

Visualization of remote RF controlled release of chemicals from the SiMNC containing, in this case, a fluorophore, (9,10-bis(phenylethynyl)anthracene) was demonstrated. The time in the figure represents the exposure time for RF (100KHz) field. The yellow region at the bottom of the UV/VIS cuvet represents the SiMNC nanocapsules with the fluorophore molecules. The liquid above the nanocapsules change color from transparent before the activation of reaction, to light green in 2 minute RF exposure, then to a well defined green color after 10 minute RF exposure.

After loading a mixture of diphenyl oxalate and fluorophore into the hollow SiMNCs using the vacuum loading process, 10 mg of chemical-trapped SiMNCs were added into the 0.5 mL solution of hydrogen peroxide followed by the exposure to an external RF magnetic field to give green fluorescence. The SiMNCs were exposed to the 100 KHz RF field to release the mixture solution of fluorophore and diphenyl oxalate into an external bath of hydrogen peroxide. The released diphenyl oxalate and hydrogen peroxide in the bath then reacted to produce phenols and the 1,2-dioxetane-3,4-dione. The latter spontaneously decomposes to carbon dioxides, releasing adequate energy to excite the fluorophore. The excited fluorophore relaxes energy states with a resultant release of photons to emit the color visualized in Fig. 30.

Chapter 3.

Study and Utilization of Magnetic Vector for Guided Tumor Penetration

3.1. Introduction

For drugs to be efficient, placement or delivery of drug-containing vehicles to the disease region is essential (*75*). For treatment of cancer, one of the major issues is the inability for effective penetration of anticancer drugs, as even small molecule drugs are able to penetrate only a few or several cell layers due to the increased abnormalities in both the vasculature and viscosity (*75, 83*). Currently no method seems to efficiently overcome such a limitation. Thus, a new technique that allows better drug penetration into cancer cell aggregates within tumors is highly desirable.

While superparamagnetic nanoparticles, such as ~10 nm diameter Fe_3O_4 magnetite, have been studied extensively for cancer treatment and drug delivery, these particles if well separated, have extremely small magnetic moment and such a very weak magnetism is not amenable for desired transport of the particles *in vitro* or *in vivo* under easily accessible magnetic fields. This poses a serious problem of difficulty in magnetic guidance as will be discussed later. Our approach has the following features: i) Hollow-

sphere nanocapsules containing intentionally trapped, closely-spaced magnetic nanoparticles, ii) defined insertion of anticancer drugs, iii) transport of these carriers by magnetic vector force (as well as by specific targeting ligands present within diseased tissues if needed), iv) controlled release of the drug cargo in an *on-off switchable* mode by remotely applied radio frequency (RF) magnetic field, and v) the continuous monitoring of carrier's traverse throughout the body via fluorescent tags. This imageable smart drug delivery system is compact because the drug molecules, magnetic nanoparticles and imaging fluorescent tags can all be self-contained within 50~150 nm capsules. The nanocapsules with closely spaced magnetic nanoparticles allow substantially increased magnetic moment to make them useful for magnetically guided transport. In the presence of a moderate gradient magnetic field, a powerful magnetic vector is created that allows these nanocapsules to cross cell membranes or blood-tissue barriers and penetrate into the midst of tumors, thus overcoming the well-known problem of limited access of anti-cancer drugs to cancer cells in the interior of a tumor tissue.

3.2. Results & Discussion

In the cancer tumor treatment, the penetration of the drug carrier into the bulky tumors, and a controlled release of the anti-cancer drugs once the drug carriers are suitably positioned in the tumors are some of the important challenges to be addressed and overcome. The former is because of the limitations of drug molecules being able to penetrate the tumor often only by a few cell thickness. The latter is for efficient use of the drug and to minimize dispensing of the often toxic drug to the unwanted regions of human body.

We have characterized the M-H magnetization loop properties of the silica-coated magnetic nanocapsules (SiMNCs) and compared with those for the superparamagnetic nanoparticles as shown in Figure 31. Compared with the same amount of loose magnetic nanoparticles with similar individual particle size (~10 nm), our silica-coated magnetic nanocapsule (SiMNC) (~80-150 nm) provide substantially improved magnetization at a high field (~x13 times at H=1T), as well as at a practical low field regime of 500~1000 Oe (~x6 times at 500 Oe), for example, at a typical applied magnetic field by small Nd-Fe-B or Sm-Co type permanent magnets placed (having a 1-2 cm dimension regime) nearby the mouse body. This enhanced magnetic strength from the nanocapsules can be attributed to the proximity and interaction of magnetic particles trapped in the capsule-confined geometry. The higher magnetization property of our silica-coated magnetic nanocapsules (SiMNCs) is important for magnetic vector enhancement for the purpose of

guiding the capsule through cell boundaries and cell cytoplasm toward the interior of the cells or deep into the midst of tumor cell aggregates. Also, DC magnetic-field-guided movement of the silica-coated magnetic nanocapsules (SiMNCs) could play an important role of enabling the nanocapsules to escape from the endosome which tends to sequester endocytosed foreign particles and make them unavailable for intended biomedical interactions.

Figure 32 schematically describes the magnet field intensity *vs* the distance from the surface of a permanent magnet, Sm-Co with a dimension of 2 cm x 2 cm area and 0.9 cm height (along the magnetized field direction). The magnetic field was measured using a gauss meter. The magnetic field gradient is estimated to be ~3,000 Oe/cm for the spacing from the magnet surface to a distance of 1 cm away. The magnetic field strength at the position of the tumor cell colony (~3 mm away from the magnet surface) is estimated to be ~2,600 Oe.

The silica-coated magnetic nanocapsules (SiMNCs) move well in an aqueous solution. For example, in the presence of ~500 Oe applied field at ~1.5 cm distance from a Sm-Co permanent magnet (see Figure 32), silica-coated magnetic nanocapsules (SiMNCs) exhibit superior magnetic vector at a movement speed of ~0.24 cm/sec. By contrast, the dispersed superparamagnetic nanoparticles with ~10 nm diameter (*84*) hardly move after many hours in the same gradient magnetic field. While the drug delivery carriers are located *in vivo* environment with a much stiffer resistance to movement than the aqueous solution environment, this data nevertheless indicate the dramatic difference in the relative mobility of the nanocapsules *vs* superparamagnetic nanoparticles.

For efficient cancer treatment, not only the drug delivery but an efficient penetration of tumor aggregates is essential. Here we utilize the powerful magnetic vector of the silica-coated magnetic nanocapsules (SiMNCs) for enhanced penetration of tumors by the drug carrier, as demonstrated in Fig. 33. The desired magnetic characteristics of such magnetic vectored nanocapsules include relatively soft magnetic properties (low coervicities to avoid/minimize nanocapsule clumping as seen in Fig. 31, blue colored M-H loop) and high saturation magnetization (so as to provide more magnetostatic pull force in gradient magnetic field for guided transport of the drug carriers). The often-researched superparamagnetic nanoparticles (e.g., ~10 nm or smaller iron oxide particles) are too weak to exert any meaningful magnetic vector force. The silica-coated magnetic nanocapsules (SiMNCs), with high concentration of magnetic nanoparticles in each nanocapsule provide much stronger magnetic moment than individual ~10 nm superparamagnetic particles.

In order to test the tumor penetration capability of our drug-containing silica-coated magnetic nanocapsules (SiMNCs), we have prepared cancer tumor colony aggregates as described in the methods section, and applied the nanocapsules for study of tumor penetration. The high-density trapped magnetic nanoparticles inside the silica shell provides our drug-containing silica-coated magnetic nanocapsules (SiMNCs) a strong penetrating vector into mouse cancer colony, for instance, under a moderate applied magnetic field of ~1,200 Oe and associated gradient field as measured and shown in Fig. 32.

In order to image and track the magnetic-field-induced movement of the magnetic nanocapsules, we attached green fluorescent tags FITC on the polystyrene sphere itself

(~100 nm diameter, containing the identical amount of magnetic nanoparticles, but before the silica shell is attached) using dextran as an intermediary functionality (*85*). Instead of fluorescent dyes, quantum dots with improved optical characteristics may also be attached as the imaging tool as demonstrated by Shi et al using Fe_3O_4-containing polystyrene surface modified with polyethylene-oxide (*86*). The field-induced movement of these FITC-attached particles without silica shells is not expected to be significantly different from that of the nanocapsules with silica shell. The gradient magnetic field was applied using a stationary magnet of either Nd-Fe-B or Sm-Co having a similar magnetic strength, for a duration of 2 hrs. The confocal microscopy images of Fig. 33 depict the penetration of these FITC-tagged nanocapsules into the cancer colony. It is clearly seen from Fig. 33, lower left image, that the nanocapsules were pulled into MT2 breast cancer cell colony using magnet gradient pulling force. The magnetic field at the equivalent distance (~8 mm) from the magnet surface to the colony is estimated to be ~1,200 Oe. The Y-Z section images (Fig. 33, left) show that the green-marker-tagged magnetic nanocapsules penetrate ~10 cell thickness cancer tumor colony toward the bottom (glass substrate) while the nanocapsules applied to the surface of the colony in the absence of applied magnet field are washed away by PBS solution during the follow-up staining process with Phalloidin-TRITC and DAPI for cell structure analysis. The confocal X-Y sections (Fig. 33, rightside images) at a location near the bottom of the colony show the presence of magnetic nanocapsules only when the gradient pulling force is applied by a magnet, but none if the magnet field is not applied.

In our in vitro observations using the cultured cancer tumor colony of ~50 μm thickness (equivalent to ~10 cell thickness), the magnetic nanocapsules powerful driving

force allowed them to penetrate through at least these ~10 cell layers of tumor tissue for the given time of 2 hrs under the magnet field, which is very encouraging for possible cancer therapeutics.

To evaluate potential applicability of our silica-coated magnetic nanocapsules (SiMNCs) for eventual *in vivo* drug delivery and efficient cancer cell treatment, the growth rates of MT2 (breast cancer cell) were evaluated *in vitro* in the presence of radio frequency (RF) activated silica-coated magnetic nanocapsules (SiMNCs) containing an anti-cancer drug. Figure 34 shows comparative growth rates (MTT assay) of MT2 mouse breast cancer cell in the presence *vs* absence of activated silica-coated magnetic nanocapsules (SiMNCs). The first bar represents the control sample with no silica-coated magnetic nanocapsule (SiMNC) present (just normal cell growth in a culture media with no capsules), while the 2nd bar represents the camptothecine-loaded silica-coated magnetic nanocapsules (SiMNCs) that have not been radio frequency (RF) activated but incubated for the same, total 40 minutes. The 3rd bar is the MTT viability data for the 8 minute x 3 times radio frequency (RF) activated camptothecine-loaded silica-coated magnetic nanocapsule (SiMNC). In the absence of applied radio frequency (RF) field, there was very little change in the viability of tumor cells between those incubated with drug-filled silica-coated magnetic nanocapsules (SiMNCs) but no radio frequency (RF) activation (the 2nd group histogram bar) *vs.* the Control (the 1st group histogram bar), as the radio frequency-field-induced drug release is the dominant event. However, with drug-filled nanocapsules remotely exposed to the radio frequency (RF) field with three 8 minute exposures with 8 minute holding periods between the exposures (the 3rd group histogram bar), a dramatic loss of tumor cell viability is seen in the cells incubated, as

shown in Figure 34. This result is quite encouraging. The on-demand radio frequency (RF) exposure caused substantially increased diffusional drug release rates (as shown in Fig. 24 and 25), which caused the much decreased viability in the cancer cells. The novelty of our system is that in the switch "off" state (without radio frequency exposure), the drug release was minimized, but in the switch "on" state (with radio frequency exposure), significant drug release occurred to maximize the therapeutic efficacy on the *in vitro* cancer cells causing a decrease in tumor viability.

In order to make sure that no unintended side effects are introduced by the experimental procedure itself, the cell viability was first tested by exposing the cells to identical radio frequency (RF) field in the absence of nanocapsules or anti-cancer drugs. There was no noticeable change in the cell viability by applying the radio frequency (RF) filed alone (data not shown). Therefore this ensures that the cell viability data was not compromised by exposure to the radio frequency (RF) field for comparable durations. Secondly, empty silica-coated magnetic nanocapsules (SiMNCs) (no drug inserted) for both cases of with vs without radio frequency (RF) exposure were provided for the viability tests. No noticeable change in MTT viability was observed in the cells incubated with empty silica-coated magnetic nanocapsules (SiMNCs) with or without radio frequency (RF) exposure (data not shown). This result implies that the presence of the nanocapsules by themselves does not induce any significant negative influence on the growth properties of tumor cells.

We have also conducted *in vivo* magnetic nanocapsule accumulation experiments using female FVB mice. When transplanted tumors (from MMTV-ErbB2 transgenic mouse) reached 1 cm in diameter, tumor-bearing mice were infused with ~$4x10^7$ silica-

coated magnetic nanocapsules (SiMNCs)/200μL PBS of FITC-tagged magnetic nanocapsules (similarly as in Fig. 34 experiments). Mice were then immobilized and treated with a magnet placed in contact with the outside skin of the mice near the tumor (estimated to be approximately a few centimeters size). After a constant magnet field (of at least ~1,000 Oe) was applied for two hours, they were euthanized and the tissue samples analyzed. The red spot in Fig.35 (a) schematically depicts the tumor site in the mice. As indicated in Fig. 35 (b), the average number of the magnetic nanocapsules trapped in the tumor cells was quite significant, i.e., ~x200 times greater with magnetic attraction as compared to that for the control group sample (magnetic nanocapsules similarly tail vein injected but no magnet field applied) for this set of *in vivo* experiments. The results of the *in vivo* magnetic capsule accumulation test are shown in Fig. 36. The FITC imaging results on surgically obtained tumor tissues show the presence of accumulated nanocapsules in the tumor tissue (green markers) for the case of the magnet placed nearby. The much higher number of magnetic nanocapsules (green) in the magnet-processed tumor samples, lower left image of Fig. 36, is apparent. The control experiment with no magnet nearby (Fig. 36, upper left) shows very few magnetic nanocapsules near the tumor site. The DAPI image shows the tumor structure via imaging of the nuclei in the tumor.

Immmuno-analysis of liver and spleen tissues was also conducted, which indicated a high efficiency of nanocapsule usage, with >~90% of the nanocapsules concentrated near the tumor cites. This result is also encouraging as the amount of wasted drug carriers can be minimized.

This Chapter, in full, has been submitted for publication, “Magnetically Vectored Nanocapsules for Tumor Penetraion and Remotely Switchable On-Demand Drug Release”, by Seong Deok Kong, Weizhou Zhang, Jun Hee Lee, Karla Brammer, Ratnesh Lal, Michael Karin, and Sungho Jin.

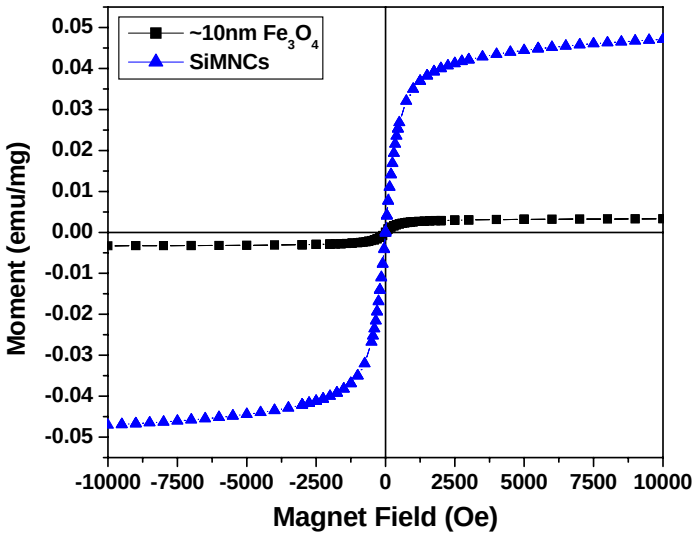

Figure 31. M-H loops showing a significant increase in magnetic moment in SiMNC configuration as compared with isolated 10 nm magnetic nanoparticles of Fe_3O_4, which allows a powerful magnetic vector for penetration of the tumor.

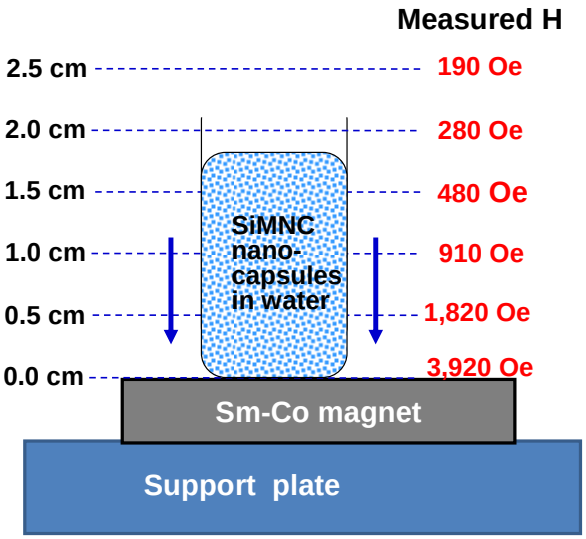

Figure 32. Measured magnetic field vs distance from the surface of a permanent magnet. Schematically describes the magnet field intensity vs the distance from the surface of a permanent magnet, Sm-Co with a dimension of 2 cm x 2 cm area and 0.9 cm height (along the magnetized field direction). The magnetic field was measured using a gaussmeter. The magnetic field gradient is estimated to be ~3,000 Oe/cm for the spacing from the magnet surface to a distance of 1 cm away. The magnetic field strength at the position of the tumor cell colony (~3 mm away from the magnet surface) is estimated to be ~2,600 Oe.

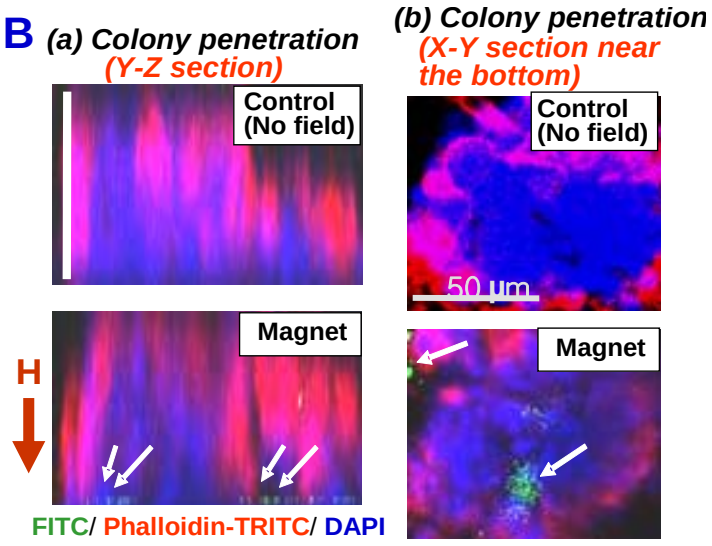

Figure 33. Confocal microscopy images of the capsule penetration into MT2 breast cancer cell colony using magnet gradient pulling force (vertical scale bar=50 μm) applied for 2 hrs by a Nd-Fe-B magnet (H=~1,200 Oe near the cancer colony location). The Y-Z and X-Y section images demonstrate a successful penetration of cancer colony by magnetic nanocapsules.

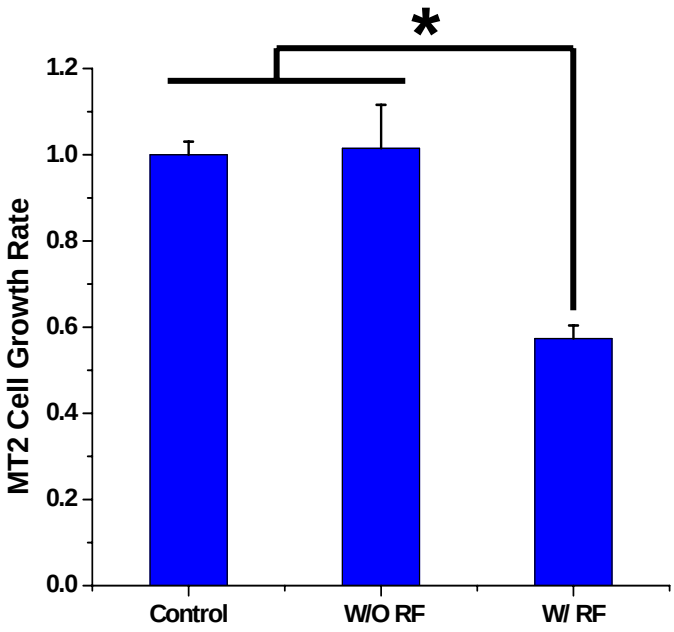

Figure 34. Comparative growth rates of MT2 cells with vs without activated SiMNCs. A significantly suppressed tumor growth is observed only when the Cpt-loaded nanocapsules are activated.

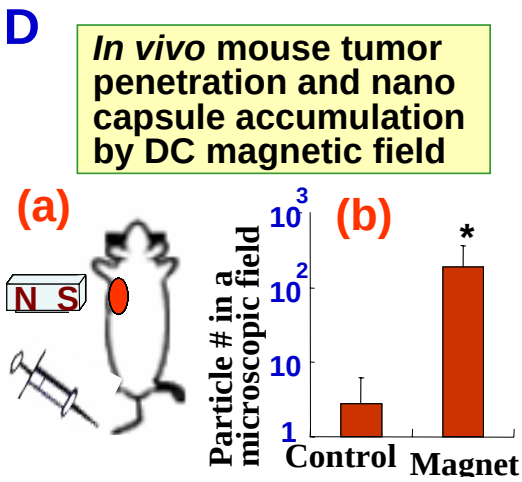

Figure 35. *In vivo* mouse tumor penetration using an external magnet near the mouse after the magnetic capsules were tail vein injected. Significantly increased number of drug-delivery-nanocapsules are retained in the tumor tissues by magnetic field processing.

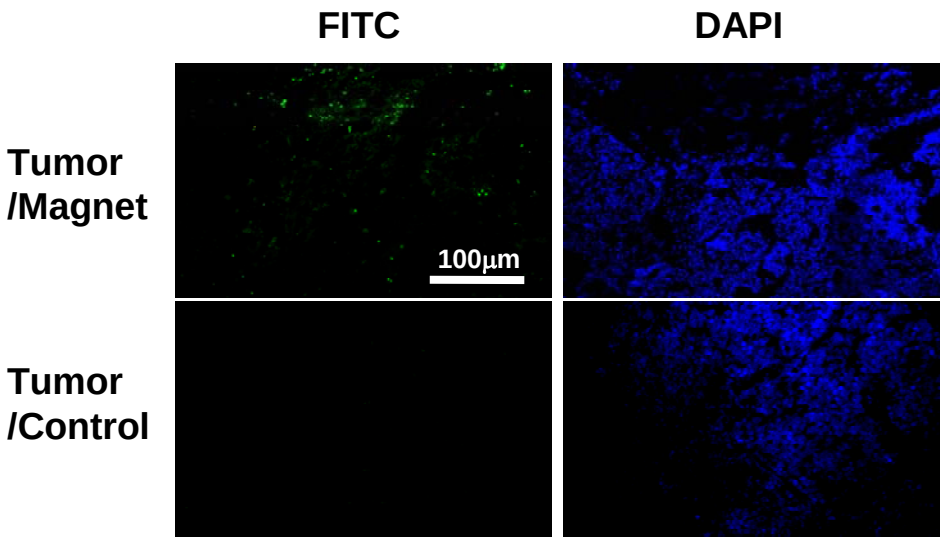

Figure 36. Imaging of i*n vivo* mouse tumor penetration in surgically obtained tumor tissues showing the drug-carrier nanocapsules (FITC green markers) due to the magnet field. Control experiment with tail vein injected SiMNCs but no magnet nearby shows very few magnetic capsules near the tumor site.

3.3. Methods

3.3.1. *In vitro* cell viability test

The cells cultivated for *in vitro* experiments were MT2 mouse mammary breast tumor cells derived from a tumor of MMTV-c-Neu Tg mice from Dr. Michael Karin's lab (University of California, San Diego, USA). MT2 cells were maintained in F12 medium (Invitrogen), supplemented with 10% fetal bovine serum, 10 ng/ml EGF, 5 μg/ml of insulin, 1μg/ml hydrocortisone, 100U/ml penicillin, and 100μg/ml of streptomycin. All cells were cultured at 37^{o}C in a 5% CO_2 and 95% air humidified atmosphere. Initially counted MT2 mouse melanoma cells were seeded into 3 plates (35x10 mm style tissue culture plates) in 2 mL of complete media and incubated overnight. The solutions exposed vs. not exposed to RF were prepared with 800 μL of PBS and 160 μg of Cpt-loaded SiMNCs. The Cpt-loaded SiMNCs was washed by 1 mL of PBS three times and then the drug release was performed with fresh 800 μL of PBS by 8 minutes of RF exposure three times with 8 minute holding periods between the exposures (the total running time was 40 minutes), which was designated as "W/ RF". For the experiment, "W/O RF" (no RF field applied for the SiMNC carriers), an equal total time of 40 minutes was used. After that, the prepared solution with the fresh 1.2 mL medium (the total volume was 2 mL.) was added to the cells. After 48 h incubation, MTT assay was performed to determine the viability of cells and normalized to cells incubated with Control.

In order to make sure that no unintended side effects are introduced by the experimental procedure itself, the cell viability was first tested by exposing the cells to identical RF field in the absence of nanocapsules or anti-cancer drugs. There was no noticeable change in the cell viability by applying the RF filed alone (data not shown). Therefore this ensures that the cell viability data was not compromised by exposure to the RF field for comparable durations. Secondly, empty SiMNCs (no drug inserted) for both cases of with *vs* without RF exposure were provided for the viability tests. No noticeable change in MTT viability was observed in the cells incubated with empty SiMNCs with or without RF exposure (data not shown). This result implies that the presence of the nanocapsules by themselves does not induce any significant negative influence on the growth properties of tumor cells.

3.3.2. Colony formation and tumors

Subconfluent MT2 cells were trypsinized and evenly resuspended at a density of $2X10^5$ cells/3 ml of F12 medium containing 0.4% Agar, antibiotics, and 7.5% fetal bovine serum. Cell suspensions were layered in 6-well dishes over a 0.7% agar base. Cells were grown at 37 °C with addition of 0.5 ml of normal medium every 3 days.

One week later, colonies were collected and seeded onto poly-L-Lysine-coated cover slips and incubated at 37 °C for overnight. The magnetic nanocapsules were applied to the 1 mL medium and incubated two hours with or without magnetic gradient force.

3.3.3. *In vivo* magnetic capsule accumulation experiments

Female FVB mice were purchased from Charles River Laboratory. Mice were anesthetized with isoflurane. The skin was incised and tumor fragments (10mg) from MMTV-ErbB2 transgenic mouse were transplanted into the #2 mammary gland at 3 months of age. When tumors reached at least 1-2 cm in diameter, tumor-bearing mice were infused with ~$4x10^7$ SiMNCs in 200μL PBS intravenously. Mice were then immobilized and treated with magnetic field of ~1,200 Oe adjacent to tumors for two hours. Control groups were not treated with magnetic field. Mice were euthanized. Livers and tumors were collected for smash preparation or frozen sections. The samples were stained with DAPI to visualize the tumor cell nuclei, and observed under epifluorescence-equipped microscope. All mice were maintained under specific pathogen-free conditions and all experimental protocols were approved by the UCSD Animal Care Program, following National Institutes of Health guidelines.

After the 2 hr exposure, the mice were euthanized. The *in vivo* magnetic capsule accumulation was tracked by fluorescence-tagged nanocapsules as shown in Fig. 35. P values after performing one-way ANOVA reaching statistical significance $P<0.01$ are marked on the graphs: * denotes significance between control and magnet.

Livers and tumors were collected for smash preparation or frozen sections. The samples were stained with FITC to image the nanocapsules and with DAPI to visualize the cancer cell nuclei, and observed under epifluorescence-equipped microscope.

Chapter 4.

Potential Applications to Blood-Brain-Barrier Crossing and Other Therapeutics

The magnetic nanocapsules developed in this research can provide a powerful magnetic vector which can be utilized for other biomedicine applications.

One of the main barriers in the central nervous system (CNS) therapeutics is the difficulty of crossing Blood-Brain-Barrier (BBB) to deliver the desired drug to the neural systems in the brain. An example of such a difficulty is for intended compound (e.g., drug) delivery by crossing the brain-blood barrier through the tight gap junctions or through endocytosis. Use of nanoparticles to enhance drug delivery across BBB has been actively pursued in recent years (*87*). A new technique to allow better drug penetration through BBB is highly desirable.

Nanoparticle based delivery is of particular interest for the central nervous system (CNS). The CNS system represents the largest part of the nerve system including the brain and the spinal cord. Almost twice as many people suffer from CNS diseases (such as Alzheimer's disease, schizophrenia, epilepsy, multiple sclerosis, stroke and brain tumors) as the cardiovascular diseases pertaining to the heart and blood vessels. However, the advances in CNS drug technology have been hindered by the inherent and unique microscale anatomy of human body, the existence of the called "Blood Brain Barrier

(BBB)". The blood brain barrier is a physiological deterrent to the introduction of unwanted large molecules to the central nervous system, with the endothelial cells overlapping tightly each other at "tight junctions". It represents a significant obstacle for delivery of a large number of drugs, including central nervous system (CNS)-active drugs, antibiotics, antineoplastic agents, and therapeutic drugs to brain tumors. An understanding of the specific mechanisms of the brain capillary endothelium has led to the development of various strategies to enhance the penetration of drugs into the brain tissue. Drug-loaded nanocarriers capable of recognizing brain capillary endothelial cells and cerebral tumoral cells by using site-specific ligands for targeting have shown promising potential in oncology. Endogenous and chimeric ligands binding to carriers or receptors of the Blood-Brain-Barrier (BBB) have been directly or indirectly conjugated to nanocarriers.

Currently, four main approaches are considered for drug transport across the Blood-Brain-Barrier (BBB): a) direct injection into intended site for drug delivery. This injection process, currently the only method used in humans, is highly efficient for drug delivery but it involves invasive procedures and requires specialist medical teams and equipment. b) Permeation through tight junctions using osmotic disruption or biochemical opening, which leads to a reversible but non-specific opening of the tight junction to allow drug transport across Blood-Brain-Barrier (BBB). c) Enhanced drug delivery through the endothelial cells (transcytosis) to the underlying brain cells by utilizing the endocytosis mechanism using liposomes or nanoparticles loaded with the drug to be delivered. This approach can be further enhanced by receptor mediated endocytosis specifically targeting the delivery system to receptors on the brain

endothelium surface. d) Use of nanoparticles to enhance drug delivery across BBB has been actively pursued in recent years. The small size of nanoparticles having functionalizable surfaces is an advantage as drug delivery carrier. However, the main problem of Blood-Brain-Barrier (BBB) still remains unsolved and remains as a serious issue. In this invention, innovative concepts have been advanced to solve the Blood-Brain-Barrier (BBB) problem as described below.

The magnetic nanocapsules designed in this research can be useful for efficient Blood-Brain-Barrier (BBB) crossing (see Fig. 37). The general approach encompasses a utilization of a gradient magnetic field guidance of the magnetic nanocapsules to specific desired neural cell regions in the brain by enable to cross the BBB (Blood-Brain-Barrier) followed by switchable drug release using radio frequency (RF) magnetic field or ultrasound activation.

Such an approach could allow extra driving force for the drug capsules to cross the Blood-Brain-Barrier (BBB) and reach the brain cells in certain desired CNS (central nervous system) regions, as illustrated in Fig. 37. Once the Blood-Brain-Barrier (BBB) is crossed, the drug capsules are activated (switched-on) by remote radio frequency (RF) magnetic field or ultrasonic activation for drug release.

The movement and heating of magnetic nanoparticles are severely deteriorated if the overall diameter is increased by polymer conjugation as a strong dependence on the size and the suspending medium is observed. Thus, the magnetic nanocapsules with a compact geometrical design, e.g., containing drug, tracer or other molecule, inside the nanosphere – and the compound's release from the inside of the nanosphere on triggerable mode would be highly desirable. The advantages of the magnetic

nanocapsules of this research is that they are compact in nature --- the compound (e.g., drug) and magnetic nanoparticles are both stored and carried within the nanospheres, thus the overall size is relatively small (~100 nm regime) which is much smaller than if the nanosphere has compound, e.g., a drug, tracer or other molecule, outside of the nanosphere.

The magnetic nanocapsules from this research can also be useful for general drug concentration enhancement at local sites as illustrated in Fig. 38. External magnet induced, position-fixed accumulation of capsules can be accomplished for preferential drug delivery to certain desirable locations followed by switchable drug release using radio frequency (RF) magnetic field or ultrasound activation.

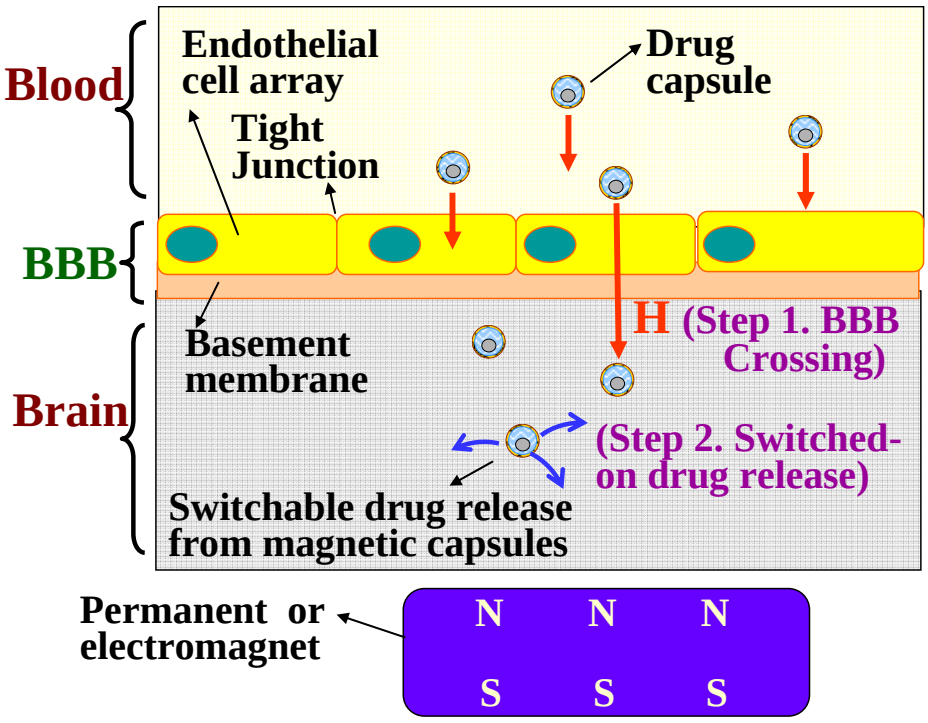

Figure 37. BBB crossing of drug-containing magnetic capsule by magnetic vector. *Step 1*. DC gradient magnetic field vector is applied for BBB crossing (through tight junction or cell membrane or via enhanced endocytosis) through the membranes. *Step 2*. Once the BBB is crossed, a high frequency AC magnetic field is applied to locally heat the magnetic capsule or induce vibration and to remotely switch-on the drug release for desired period and regimen.

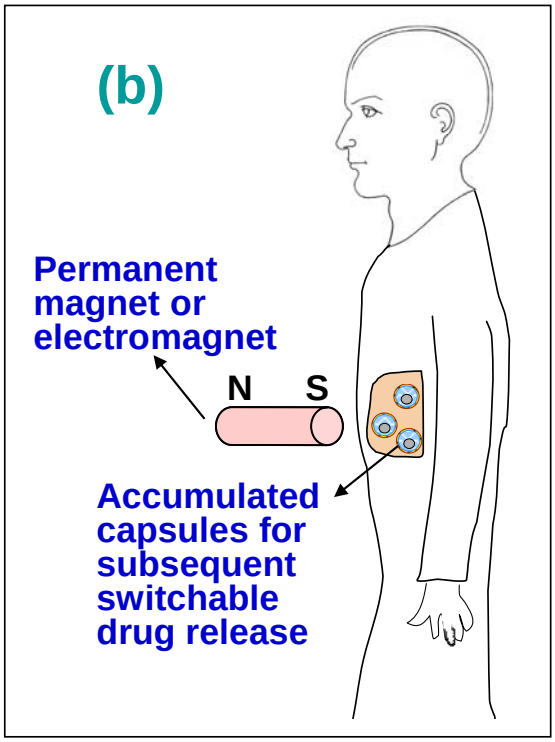

Figure 38. Magnetic position fixing of accumulation of drug capsules and subsequent drug release by RF field or ultrasonic activation. A slow dragging movement of magnets to relocate the accumulated drug capsules is also possible.

Chapter 5.

Conclusion

The synthesis, magnetic movement and remote, on-off switchable drug delivery of magnetic nanocapsules, as well as their guided cancer colony penetration have been investigated in this research. The results in this dissertation clearly show a simple but powerful way of targeted drug delivery to the tumors by using remotely activated, anticancer-drug-loaded magnetic nanocapsules. Our on-off switchable, nanocapsules have the advantages of allowing defined insertion of hydrophobic or hydrophilic anti-cancer drugs, exhibit a *powerful magnetic vector* to penetrate into the midst of tumors, followed by remotely activated, on-demand release of anti-cancer drugs, thus offering a promise of overcoming the well-known problem of limited access of anti-cancer drugs to the desired location in the interior of tumor tissues. The nanocapsules tagged with fluorescent markers allow continuous monitoring of the drug carrier transport.

The magnetic nanocapsules of this research can also be useful for other biomedical applications including treatments for many types of cancers, drug delivery to various specific organs within the human body, and for efficient blood-brain-barrier (BBB) crossing, which may have a huge impact for central nervous system (CNS) therapeutics.

References

1. K. K. Jain, *Methods Mol Biol* **437**, 1 (2008).

2. T. M. Allen, P. R. Cullis, *Science* **303**, 1818 (Mar 19, 2004).

3. T. M. Allen, *Nat Rev Cancer* **2**, 750 (Oct, 2002).

4. J. Huwyler, D. Wu, W. M. Pardridge, *Proc Natl Acad Sci U S A* **93**, 14164 (Nov 26, 1996).

5. R. K. Chowdhary, I. Shariff, D. Dolphin, *J Pharm Pharm Sci* **6**, 13 (Jan-Apr, 2003).

6. H. Maeda, J. Wu, T. Sawa, Y. Matsumura, K. Hori, *J Control Release* **65**, 271 (Mar 1, 2000).

7. D. A. LaVan, T. McGuire, R. Langer, *Nat Biotechnol* **21**, 1184 (Oct, 2003).

8. X. Guo, F. C. Szoka, Jr., *Acc Chem Res* **36**, 335 (May, 2003).

9. O. C. Farokhzad, R. Langer, *Acs Nano* **3**, 16 (Jan, 2009).

10. A. D. Bangham, M. M. Standish, J. C. Watkins, *Journal of Molecular Biology* **13**, 238 (1965).

11. R. Langer, J. Folkman, *Nature* **263**, 797 (1976).

12. M. B. Yatvin, W. Kreutz, B. A. Horwitz, M. Shinitzky, *Science* **210**, 1253 (1980).

13. L. D. Leserman, J. Barbet, F. Kourilsky, J. N. Weinstein, *Nature* **288**, 602 (1980).

14. T. D. Heath, R. T. Fraley, D. Papahadjopoulos, *Science* **210**, 539 (1980).

15. T. M. Allen, A. Chonn, *Febs Letters* **223**, 42 (Oct 19, 1987).

16. A. L. Klibanov, K. Maruyama, V. P. Torchilin, L. Huang, *Febs Letters* **268**, 235 (Jul 30, 1990).

17. R. Gref *et al.*, *Science* **263**, 1600 (Mar 18, 1994).

18. C. S. Brazel, *Pharm Res* **26**, 644 (Mar, 2009).

19. T. Y. Liu, S. H. Hu, T. Y. Liu, D. M. Liu, S. Y. Chen, *Langmuir* **22**, 5974 (Jul 4, 2006).

20. S. H. Hu, T. Y. Liu, D. M. Liu, S. Y. Chen, *Macromolecules* **40**, 6786 (Sep 18, 2007).

21. N. Butoescu, O. Jordan, A. Petri-Fink, H. Hofmann, E. Doelker, *Journal of Microencapsulation* **25**, 339 (2008).

22. J. Dobson, S. H. Cartmell, A. Keramane, A. J. El Haj, *Ieee Transactions on Nanobioscience* **5**, 173 (Sep, 2006).

23. D. E. Discher *et al.*, *Progress in Polymer Science* **32**, 838 (Aug-Sep, 2007).

24. Y. C. Chang, S. W. Chang, D. H. Chen, *Reactive & Functional Polymers* **66**, 335 (Mar, 2006).

25. D. H. Kim, D. E. Nikles, D. T. Johnson, C. S. Brazel, *Journal of Magnetism and Magnetic Materials* **320**, 2390 (Oct, 2008).

26. C. S. Brazel, N. A. Peppas, *Journal of Controlled Release* **39**, 57 (Mar, 1996).

27. A. Chilkoti, M. R. Dreher, D. E. Meyer, D. Raucher, *Advanced Drug Delivery Reviews* **54**, 613 (Sep 13, 2002).

28. A. K. Gupta, M. Gupta, *Biomaterials* **26**, 3995 (Jun, 2005).

29. R. K. Gilchrist *et al.*, *Ann Surg* **146**, 596 (Oct, 1957).

30. V. S. Kalambur, B. Han, B. E. Hammer, T. W. Shield, J. C. Bischof, *Nanotechnology* **16**, 1221 (Aug, 2005).

31. S. Mornet, S. Vasseur, F. Grasset, E. Duguet, *Journal of Materials Chemistry* **14**, 2161 (2004).

32. S. R. Dave, X. H. Gao, *Wiley Interdisciplinary Reviews-Nanomedicine and Nanobiotechnology* **1**, 583 (Nov-Dec, 2009).

33. K. M. Krishnan *et al.*, *Journal of Materials Science* **41**, 793 (Feb, 2006).

34. C. Z. Simonsen *et al.*, *Journal of Magnetic Resonance Imaging* **9**, 342 (Feb, 1999).

35. D. L. J. Thorek, A. Chen, J. Czupryna, A. Tsourkas, *Annals of Biomedical Engineering* **34**, 23 (Jan, 2006).

36. M. A. Lopez-Quintela, C. Tojo, M. C. Blanco, L. G. Rio, J. R. Leis, *Current Opinion in Colloid & Interface Science* **9**, 264 (Nov, 2004).

37. Y. Lee *et al.*, *Advanced Functional Materials* **15**, 503 (Mar, 2005).

38. J. Park *et al.*, *Angewandte Chemie-International Edition* **44**, 2872 (2005).

39. Y. Lu, Y. D. Yin, B. T. Mayers, Y. N. Xia, *Nano Letters* **2**, 183 (Mar, 2002).

40. N. Murthy, J. R. Robichaud, D. A. Tirrell, P. S. Stayton, A. S. Hoffman, *Journal of Controlled Release* **61**, 137 (Aug 27, 1999).

41. Y. W. Jun *et al.*, *Journal of the American Chemical Society* **127**, 5732 (Apr 27, 2005).

42. D. Artemov, N. Mori, B. Okollie, Z. M. Bhujwalla, *Magnetic Resonance in Medicine* **49**, 403 (Mar, 2003).

43. R. Weissleder, U. Mahmood, *Radiology* **219**, 316 (May, 2001).

44. J. M. Perez, L. Josephson, R. Weissleder, *Chembiochem* **5**, 261 (Mar 5, 2004).

45. J. M. Perez, L. Josephson, T. O'Loughlin, D. Hogemann, R. Weissleder, *Nature Biotechnology* **20**, 816 (Aug, 2002).

46. J. H. Lee *et al.*, *Nature Medicine* **13**, 95 (Jan, 2007).

47. Y. M. Huh *et al.*, *Journal of the American Chemical Society* **127**, 12387 (Sep 7, 2005).

48. B. K. Oh, J. M. Nam, S. W. Lee, C. A. Mirkin, *Small* **2**, 103 (Jan, 2006).

49. J. M. Nam, K. J. Jang, J. T. Groves, *Nature Protocols* **2**, 1438 (2007).

50. J. Yang *et al.*, *Journal of Materials Chemistry* **17**, 2695 (2007).

51. M. W. Wilson *et al.*, *Radiology* **230**, 287 (Jan, 2004).

52. A. S. Lubbe, C. Bergemann, J. Brock, D. G. McClure, *Journal of Magnetism and Magnetic Materials* **194**, 149 (Apr, 1999).

53. J. Kim *et al.*, *Advanced Materials* **20**, 478 (Feb 4, 2008).

54. Z. Medarova, W. Pham, C. Farrar, V. Petkova, A. Moore, *Nature Medicine* **13**, 372 (Mar, 2007).

55. C. T. Kresge, M. E. Leonowicz, W. J. Roth, J. C. Vartuli, J. S. Beck, *Nature* **359**, 710 (Oct 22, 1992).

56. J. S. Beck *et al.*, *Journal of the American Chemical Society* **114**, 10834 (Dec 30, 1992).

57. M. Vallet-Regi, A. Ramila, R. P. del Real, J. Perez-Pariente, *Chemistry of Materials* **13**, 308 (Feb, 2001).

58. P. Horcajada, A. Ramila, J. Perez-Pariente, M. Vallet-Regi, *Microporous and Mesoporous Materials* **68**, 105 (Mar, 2004).

59. A. Stein, B. J. Melde, R. C. Schroden, *Advanced Materials* **12**, 1403 (Oct 2, 2000).

60. M. Vallet-Regi, *Chemistry-a European Journal* **12**, 5934 (Aug 7, 2006).

61. A. G. Cuenca *et al.*, *Cancer* **107**, 459 (Aug 1, 2006).

62. D. A. Groneberg, M. Giersig, T. Welte, U. Pison, *Current Drug Targets* **7**, 643 (Jun, 2006).

63. S. Jin, K. M. Ye, *Biotechnology Progress* **23**, 32 (Jan-Feb, 2007).

64. V. Roy, E. A. Perez, *Seminars in Oncology* **33**, S3 (Jun, 2006).

65. A. Beduneau, P. Saulnier, J. P. Benoit, *Biomaterials* **28**, 4947 (Nov, 2007).

66. Y. K. a. T.Okano, *Temperature responsive hydrogels as intelligent materials, Chap.2, Biorelated Polymers and Gels*. T. Okano, Ed. (Academic Press, New York, 1998), pp.

67. K. Sawahata, M. Hara, H. Yasunaga, Y. Osada, *Journal of Controlled Release* **14**, 253 (1990).

68. J. Kost, J. Wolfrum, R. Langer, *Journal of Biomedical Materials Research* **21**, 1367 (1987).

69. T. Shimoboji *et al.*, *Proceedings of the National Academy of Sciences of the United States of America* **99**, 16592 (2002).

70. S. M. Henry, M. E. H. El-Sayed, C. M. Pirie, A. S. Hoffman, P. S. Stayton, *Biomacromolecules* **7**, 2407 (2006).

71. T. Hoare *et al.*, *Nano Letters* **9**, 3651 (Oct, 2009).

72. J. T. Santini, M. J. Cima, R. Langer, *Nature* **397**, 335 (Jan 28, 1999).

73. Y. Li *et al.*, *J Control Release* **100**, 211 (Nov 24, 2004).

74. K. E. Uhrich, S. M. Cannizzaro, R. S. Langer, K. M. Shakesheff, *Chemical Reviews* **99**, 3181 (1999).

75. S. H. Jang, M. G. Wientjes, D. Lu, J. L. Au, *Pharm Res* **20**, 1337 (Sep, 2003).

76. B. Tasdelen, N. Kayaman-Apohan, O. Guven, B. M. Baysal, *Radiation Physics and Chemistry* **73**, 340 (Aug, 2005).

77. Y. Yin *et al.*, *Science* **304**, 711 (Apr 30, 2004).

78. Y. G. Sun, B. T. Mayers, Y. N. Xia, *Nano Letters* **2**, 481 (May, 2002).

79. S. W. Kim, M. Kim, W. Y. Lee, T. Hyeon, *Journal of the American Chemical Society* **124**, 7642 (Jul 3, 2002).

80. H. P. Liang, L. J. Wan, C. L. Bai, L. Jiang, *Journal of Physical Chemistry B* **109**, 7795 (Apr 28, 2005).

81. H. Xu, L. Cui, N. Tong, H. Gu, *J Am Chem Soc* **128**, 15582 (Dec 13, 2006).

82. J. Yang, J. U. Lind, W. C. Trogler, *Chemistry of Materials* **20**, 2875 (May 13, 2008).

83. D. Fukumura, R. K. Jain, *Apmis* **116**, 695 (2008).

84. T. R. Pisanic, J. D. Blackwell, V. I. Shubayev, R. R. Finones, S. Jin, *Biomaterials* **28**, 2572 (Jun, 2007).

85. Z. Yu, W. Xiaoliang, W. Xuman, X. Hong, G. Hongchen, *J Biomed Mater Res A* **85**, 582 (Jun 1, 2008).

86. D. L. Shi *et al.*, *Advanced Materials* **21**, 2170 (Jun 5, 2009).

87. W. M. Pardridge, *Current Opinion in Pharmacology* **6**, 494 (Oct, 2006).